

Contrastive Tuning: A Little Help to Make Masked Autoencoders Forget

Johannes Lehner^{* 1}Benedikt Alkin^{* 1}Andreas Fürst¹Elisabeth Rumetshofer¹Lukas Miklautz^{† 2 3}Sepp Hochreiter^{1 4}

Abstract

Masked Image Modeling (MIM) methods, like Masked Autoencoders (MAE), efficiently learn a rich representation of the input. However, for adapting to downstream tasks, they require a sufficient amount of labeled data since their rich features capture not only objects but also less relevant image background. In contrast, Instance Discrimination (ID) methods focus on objects. In this work, we study how to combine the efficiency and scalability of MIM with the ability of ID to perform downstream classification in the absence of large amounts of labeled data. To this end, we introduce Masked Autoencoder Contrastive Tuning (MAE-CT), a sequential approach that applies Nearest Neighbor Contrastive Learning (NNCLR) to a pre-trained MAE. MAE-CT tunes the rich features such that they form semantic clusters of objects without using any labels. Applied to large and huge Vision Transformer (ViT) models, MAE-CT matches or excels previous self-supervised methods trained on ImageNet in linear probing, k -NN and low-shot classification accuracy as well as in unsupervised clustering accuracy. Notably, similar results can be achieved without additional image augmentations. While ID methods generally rely on hand-crafted augmentations to avoid shortcut learning, we find that nearest neighbor lookup is sufficient and that this data-driven augmentation effect improves with model size. MAE-CT is compute efficient. For instance, starting from a MAE pre-trained ViT-L/16, MAE-CT increases the ImageNet 1% low-shot accuracy from 67.7% to 72.6%, linear probing accuracy from 76.0% to 80.2% and k -NN accuracy from 60.6% to 79.1% in just five hours using eight A100 GPUs.

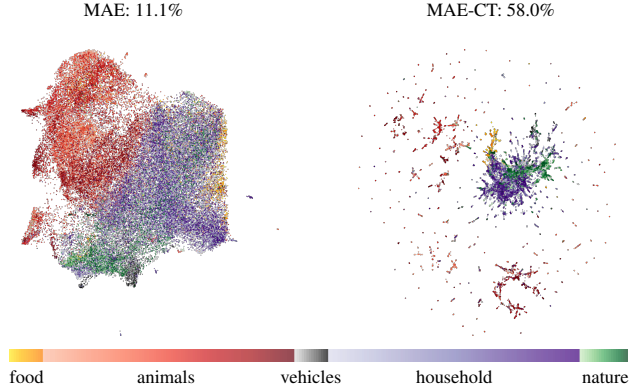


Figure 1. Formation of clusters induced by Masked Autoencoder Contrastive Tuning (MAE-CT). MAE leads to a coarse clustering of objects, in the form of ImageNet super-classes, like food, animals, vehicles, household objects, or objects in nature, that summarize several classes. MAE-CT forms object-specific clusters and thereby improves the k -means cluster accuracy w.r.t. the 1000 ImageNet ground truth classes from 11.1% to 58.0% without additional image augmentations or labeled data.

1. Introduction

Self-supervised representation learning aims at constructing rich representations of the input without explicit supervision from costly annotated labels. Therefore, self-supervised learning is currently one of the most effective machine learning concepts. In computer vision, the two main streams of self-supervised learning are Instance Discrimination (ID; e.g. [38, 17, 62, 35, 13, 88, 8]) and Masked Image Modeling (MIM; e.g. [7, 37, 84, 6]).

We combine these two approaches and present Masked Autoencoder Contrastive Tuning (MAE-CT). A training procedure that builds on the efficiency, scalability and generality of Masked Autoencoders (MAEs; [37]). MAE-CT extends MAE with the ability of ID methods to abstract from background details and to form object-specific clusters (w.r.t. human given labels) in the encoder representations. MAE-CT first trains a rich MAE model and, subsequently, performs contrastive tuning (CT) with the Nearest Neighbor Contrastive Learning (NNCLR; [29]) objective.

^{*} Equal contribution [†] Main work conducted during research stay

¹ ELLIS Unit Linz and LIT AI Lab, Institute for Machine Learning Johannes Kepler University, Linz, Austria

² Faculty of Computer Science, University of Vienna, Vienna, Austria

³ UniVie Doctoral School Computer Science, University of Vienna

⁴ Institute of Advanced Research in Artificial Intelligence (IARAI)

Corresp. to {alkin, lehner}@ml.jku.at, lukas.miklautz@univie.ac.at

Code available at <https://github.com/ml-jku/MAE-CT>

MAE-CT abstracts features of pre-trained MAEs, that encode object-irrelevant details, to object-specific features. MAE-CT does not require label supervision or additional image augmentations besides the crop and flip augmentations already used in MAE pre-training.

We provide the following contributions:

1. We introduce MAE-CT which combines the advantages of MIM and ID. MAE-CT is data efficient and scalable like MAEs, while learning abstract and clustered input representations like contrastive methods that yield a better initial object description (UMAP [60] plots in Figure 1). MAE-CT matches or surpasses the performance of ID methods trained on ImageNet in linear probing, k -NN and low-shot classification accuracy as well as in unsupervised clustering accuracy.
2. We provide empirical evidence that the data-driven augmentation effect induced by the nearest neighbor (NN) lookup of NNCLR benefits from larger models. Consequently, the performance gap to a version that uses hand-crafted augmentations becomes smaller when we scale the model size. Furthermore, we find that sampling from the top- k -NN increases augmentation strength and improves clusters in the embedding.
3. We explore end-to-end training of MAE together with NNCLR. We find that, without additional augmentations combined training compares unfavorable to the more flexible sequential approach. We conduct experiments to estimate the degree of shortcut learning [33], which increases in the combined version.

2. Background

Instance discrimination (ID). First, ID methods generate different views of the same image via augmentations. Then, they align the representations of these views in order to obtain representations that are invariant to the transformations that generated the views [75]. A trivial solution for alignment would be a constant representation, which corresponds to an undesired collapse of the representation space to a single point. Representation collapses can be avoided in different ways: (a) contrastive methods [43, 38, 17, 62] rely on a loss that penalizes the similarity to views of other samples, the so-called negatives; (b) teacher-student approaches [35, 13, 18] prevent collapses via an asymmetry between an active student and a teacher; (c) various methods circumvent collapses by constraints that rely on clustering [10, 11] or on invariances [88, 8]. Typically, ID methods learn object-specific representations that are suited to solve downstream classification tasks with a linear or k -nearest neighbor (k -NN) classifier.

Masked Image Modeling (MIM). MIM uses a pre-training task where missing or corrupted parts of the input image have to be reconstructed.

Neither early image in-painting methods [27, 65] nor the adaptation of masked language modeling [26] in computer vision [15] achieved the performance of supervised pre-training. In computer vision, masking methods were revived by the introduction of the Vision Transformer (ViT; [28]). Due to their missing inductive biases, ViTs struggle to learn local features with limited data [67]. Furthermore, in contrast to convolutional neural networks, the ViT architecture readily enables to mask out patches without introducing undesired artifacts.

Various methods have shown that MIM can improve data efficiency and allows scaling of the model size [7, 37, 84, 6]. On smaller datasets, enhancing contrastive methods by MIM was beneficial [30]. Furthermore, masking the input of the student network has been used to improve the performance of self-distillation methods [91, 3].

Masked self-supervised learning is a very general concept and, therefore, can be applied to various domains such as natural language processing [26], audio processing [46, 53], or computer vision [37, 7, 15, 84]. However, MIM pre-training often does not create features that are suited for downstream tasks such as classification via linear probing or k -NN. Typically, downstream tasks require object-focused features while MIM mainly constructs features that are more general and allow to capture the image background. For example, MAEs must represent the image background to achieve a low reconstruction error. Therefore, adaptation mechanisms such as end-to-end fine-tuning must be applied to achieve optimal performance on downstream tasks. These adaptation mechanisms rely on hand-crafted data augmentations [37], such as RandAugment [22], Mixup [89], Cutmix [87], and other regularization techniques [45, 20].

Contrastive and clustering methods. Clustering-based contrastive methods [54, 10, 11, 13] leverage group information in the form of clusters or prototypes to avoid splitting objects that belong to the same semantic class. Therefore, these methods create object-focused features, which leads to clusters of objects of the same type or even clusters of different views of the same object. However, clustering is prone to early over-generalization by considering an entire cluster as positive examples before a proper discrimination of samples is possible [29]. This phenomenon is known in the deep clustering literature [92], in which a two step approach was shown to avoid over-generalization and trivial solutions [10, 83, 50]. First, pre-training via a self-supervised method learns a suitable representation. Subsequently, samples are clustered starting from the learned representation, thereby the model is fine-tuned to induce better

separation. The two step approach can also be implemented as a joint [83] or an alternating [85] procedure.

Similar to our approach, many deep clustering methods use autoencoders for pre-training [92], since they are more generally applicable than contrastive methods. However, their reconstruction objective generates features that do not fit to the discriminative nature of clustering or classification tasks which need object-focused features [31, 61].

To explain the success of contrastive learning, some work considers the connection between clustering and contrastive methods [64, 70, 36, 16], with recent work [2] pointing to a connection to the k -means algorithm [58, 56].

Masked Autoencoder (MAE). MAE [37] is a popular MIM method, as it enables the training of large ViT models on small datasets with reduced computational cost. During pre-training, a larger ViT model serves as an encoder and a smaller ViT model as a decoder of a Denoising Autoencoder [78]. The latter regresses the missing patches. The high masking ratio shortens the sequence length processed in the encoder, which vastly reduces the computational cost of pre-training. MAEs exhibit strong performance when fine-tuned on computer vision downstream tasks, such as object detection or instance segmentation [55, 44], and also on other modalities such as audio [46] or video [32, 76].

Nearest Neighbor Contrastive Learning (NNCLR). NNCLR [29] extends the popular contrastive method SimCLR [17] with a Nearest Neighbor (NN) lookup. Instead of calculating the InfoNCE loss between an anchor sample of one view and a positive sample of the other view, the feature vector of the positive sample is replaced by its nearest neighbor from a queue containing feature vectors of previous samples. The queue is implemented via a shift register (similar to MoCo [38]). Additionally, NNCLR adopts the asymmetric head design of BYOL [35].

When restricted to only crop and flip augmentations, NNCLR shows promising resilience to shortcut learning [33]. In an experiment with reduced training duration, NNCLR reports a relative drop of only 2.1% in linear probing performance with ResNet50 [39]. For comparison, other ID methods report a relative drop of $\sim 13\%$ (BYOL [35]), $\sim 27\%$ (Barlow Twins [88]), or $\sim 28\%$ (SimCLR [17]) in performance.

3. Method

“An autoencoder wants to remember everything a classifier wants to forget.” [31]

Motivation. MIM approaches are able to train large ViT-models, that lack the inductive bias of convolutional neural

networks, and learn rich representations from ImageNet only [37, 6, 84, 72]. However, MIM models rely on adaptation to the downstream tasks using supervised training where downstream performance heavily degrades as the number of labeled samples decreases. Conversely, ID methods suffer less from this problem as their objective implicitly forms object-specific representations during pre-training. This makes the transition to the downstream task easier as the embedding already represents similar objects in a similar way. The difference in structure can also be seen by evaluating the embedding directly via linear probing or k -NN classification where ID performs significantly better than MIM. Additionally, MAE-CT is motivated by the reported effectiveness of partial fine-tuning. Partial fine-tuning improves classification performance considerably by retraining only a few of the topmost layers in a pre-trained MAE with a supervised objective. This implies that features in the lower layers of a pre-trained MAE model already generalize well and that only upper layers need to be tuned. Further, fine-tuning induces an object-specific clustering in the representation of the MAE due to label supervision and achieves invariance to certain input features using a set of extensive input augmentations based on expert domain knowledge. Finally, fine-tuning adjusts the model from masked inputs used during MAE pre-training to unmasked inputs which are used in downstream tasks.

Overview. MAE-CT is a sequential approach to improve the abstraction of the representation of a pre-trained MAE without the need for labeled data or the introduction of additional input augmentations. MAE-CT builds on the object-focused clusters, that form in the representation of the contrastive method NNCLR, to emulate effects of fine-tuning in a self-supervised manner. We find that it is possible to achieve a far higher k -NN accuracy within the embedding of an NNCLR head than in the embedding of a pre-trained MAE encoder. This initial gap in cluster quality is essential to take full advantage of contrastive tuning, as it immediately provides a useful training signal and enables the use of stronger latent space augmentation by using one of the k nearest neighbors (instead of *the* nearest neighbor) from the queue as positive sample for the NNCLR objective. Contrastive tuning subsequently retrains the upper half of the MAE by optimizing the NNCLR objective (Figure 2, right) to form object-specific clusters in the embedding of the encoder. MAE-CT does not require the introduction of additional input augmentations. Furthermore, MAE-CT can adjust the model to the unmasked inputs used in downstream tasks. MAE-CT leads to a compact clustering of objects and enables the MAE encoder to *forget* about pre-training specific details and focus on objects within images.

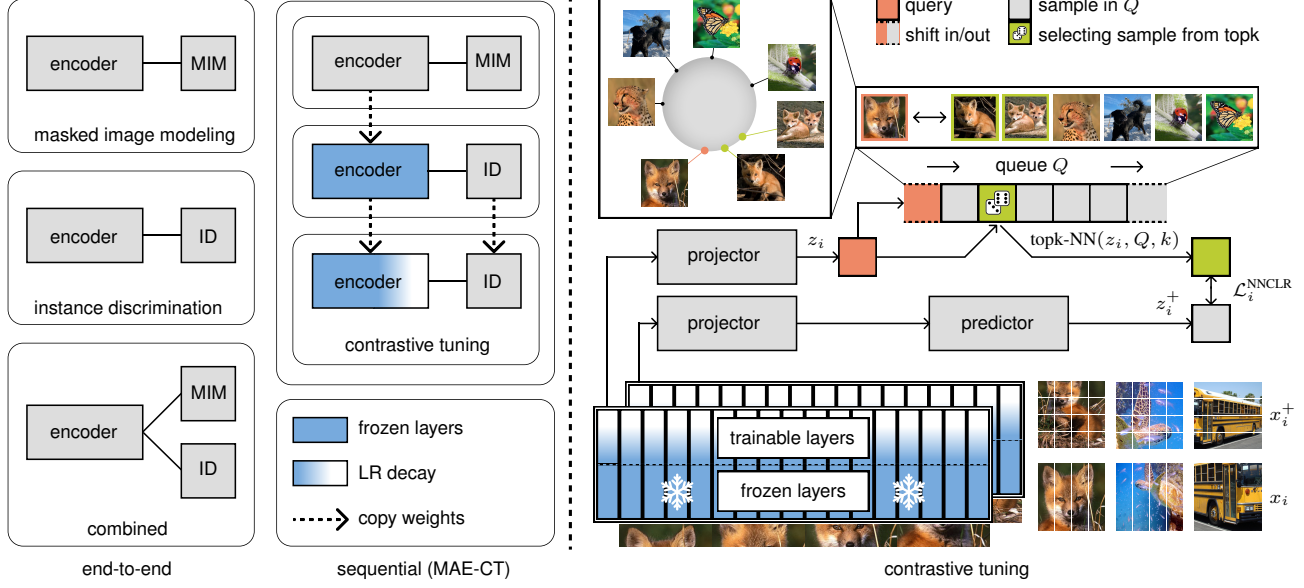


Figure 2. Contrary to end-to-end methods, MAE-CT is a sequential approach, as depicted on the left side. To prepare the components for contrastive tuning, first an encoder is pre-trained with a MIM objective (MAE). Afterwards, a NNCLR head is initialized on top of said pre-trained encoder by freezing the encoder and training the NNCLR head until its latent space representation is well structured. Finally, contrastive tuning is applied for a short duration. In contrastive tuning, depicted on the right side, we freeze the bottom half of the ViT-encoder and apply a layer-wise learning rate decay for the top half. Two views of one image are generated and then encoded by the ViT. Both encodings are fed into a projector, followed by either a predictor or a topk-NN lookup resulting in the embeddings for the NNCLR loss. The queue Q is updated with the new embeddings in a first in – first out manner after each gradient update step.

3.1. MAE pre-training & NNCLR initialization

As shown on the right side of Figure 2, contrastive tuning requires a MAE pre-trained encoder and a NNCLR head that is initialized on the output of said encoder embeddings. Thus, MAE pre-training is followed by a short training of a NNCLR head on top of the fully frozen pre-trained encoder.

3.2. Contrastive tuning

Contrastive tuning uses the initialized NNCLR head to retrain the *partially frozen* encoder. Training is performed on *unmasked* images. The NNCLR head consists of a projector, a predictor and a queue Q as shown in the right part of Figure 2. For the i -th image in a mini-batch of size n , two views x_i and x_i^+ are created by applying stochastic augmentations. Both views are propagated through the encoder. The encoder output of the first view is propagated through the projector (z_i) while the second view is propagated through the projector and the predictor (z_i^+). z_i and z_i^+ are both normalized to length 1. After each gradient update step, the queue Q is then updated with z_i from the current batch in a first in – first out manner, meaning that the oldest samples are pushed out to make space for the new ones. Instead of using z_i directly in the contrastive loss, it is replaced with one of its k nearest neighbors from Q . We refer to this augmentation procedure as topk-NN lookup.

$$\text{topk-NN}(z_i, Q, k) = \mathcal{U}_{\{1, \dots, k\}} \left(\text{topk } z_i \cdot q \right) \quad (1)$$

Using the temperature τ , we then obtain the loss function

$$\mathcal{L}_i^{\text{NNCLR}} = -\log \frac{\exp(\text{topk-NN}(z_i, Q, k) \cdot z_i^+ / \tau)}{\sum_{j=1}^n \exp(\text{topk-NN}(z_i, Q, k) \cdot z_j^+ / \tau)} \quad (2)$$

Contrary to an ablation study performed in [29], we find that topk-NN lookup improves performance. We argue that this is enabled by the high quality of the initialized NNCLR latent representation on top of the pre-trained MAE features. Consequently, we can adjust the strength of the augmentation effect by using a higher value for k .

4. Experiments and Analysis

4.1. Implementation details

MAE pre-training. For MAE pre-training, we closely follow the original procedure [37]. We train a standard ViT as encoder where 75% of the input patches are removed from the input sequence. We train for 1600 epochs with a learning rate of $1.5e-4$ and use the “normalize pixels” variant of the MAE loss, which applies a patch-wise normalization to the target pixels before the mean-squared-error loss.

NNCLR initialization. Following [29], we use a 3-layer MLP as projector, a 2-layer MLP as predictor and a queue Q of length 65536. To initialize the NNCLR-head, we train for 20 epochs on the output of the fully frozen pre-trained MAE encoder with a learning rate of $1e-4$, a temperature parameter τ of 0.15 and the default top1-NN lookup.

Contrastive tuning. We use a learning rate of $1e-4$ and apply layer-wise learning rate decay [20] with a decay factor of 0.65 to the upper half of the ViT blocks while freezing the lower half (as depicted in Figure 2, right). For MAE-CT, we train ViT-B/L for 20 epochs and ViT-H for 30 epochs. For MAE-CT_{aug} we train ViT-B for 80 epochs and ViT-L/H for 40 epochs. Further details are in Appendix A.2.

4.2. Evaluation

We evaluate our approach through image classification on ImageNet [24], where we vary the number of used labels from 100% down to a single label per class. To ensure a fair comparison, we exclude results that are based on additional training data or larger sequence lengths (via higher input resolution or smaller patch size) and provide a detailed comparison in Appendix Table 18. MAE-CT uses only minimal image augmentations, but we also evaluate our approach using the same augmentations as in BYOL [35], which are commonly used in ID methods [13, 3, 88, 19, 91]. We refer to this setting as MAE-CT_{aug}.

We choose the evaluation protocol based on the number of available labels in accordance to previous works. For evaluating the representation using 100% of the labels, we train a linear probe and a k -NN classifier. With 10% and 1% of the labels, we fine-tune the encoder and in the extreme low-shot settings (<1% labels), we report the accuracy of a logistic regression classifier averaged over three splits. The detailed protocols can be found in Appendix A.3.

4.3. Results

ImageNet linear classification. Table 1 shows the linear probing performance on the ImageNet benchmark. When restricting methods to minimal image augmentations, MAE-CT shows consistent improvements over MAE and I-JEPA [4] for all model sizes. In comparison to state-of-the-art ID methods, that use extensive image augmentations and are generally more parameter-efficient than MIM methods, MAE-CT_{aug} shows the superior scaling behavior. While self-distillation ID methods (iBOT [91], MSN [3]) using multi-crop training and extensive image augmentations [12] can achieve high performances on ViT-B/16, MAE-CT_{aug} surpasses both methods already when a ViT-L/16 model is used. The efficiency of MAE-CT allows us to scale the model size up to ViT-H. Additionally, the gap between minimal image augmentations and extensive image augmentations is shrinking with increased model size.

Method	B/16	L/16	H/14
<i>Minimal image augmentations</i>			
SimMIM [84]	56.7	-	-
MAE [37]	68.0	76.0	77.2
I-JEPA [4]	72.9	77.5	79.3
MAE-CT	73.5	80.2	81.3
<i>Extensive image augmentations</i>			
MoCo v3 [19]	76.7	77.6	79.1
MSN [3]	77.7	77.3	-
iBOT [91]	79.5	81.0	-
Layer Grafting [51]	77.7	81.0	-
MAE-CT _{aug}	76.9	81.5	82.0

Table 1. Linear probing accuracy on ImageNet. MAE-CT outperforms other methods in the setting of minimal image augmentations. When using extensive image augmentations, self-distillation ID methods are able to use of the limited parameters in of a ViT-B/16 more efficiently. Due to the superior scaling ability, MAE-CT_{aug} outperforms other methods for ViT-L/16 and ViT-H/14.

Low-shot evaluation. Table 2 shows classification accuracy when using only a fraction of the labels. Similar to linear probing, MAE-CT_{aug} shows superior scaling as it outperforms state-of-the-art ID methods on larger model scales. While extensive augmentations are superior for smaller models (ViT-B/16) and more labels (10%), they become less effective as model size grows and the number of labels decreases. For ViT-L/16 models, MAE-CT surpasses the performance of methods that use extensive augmentations on the 1 shot and 2 shot benchmark. Similarly, MAE-CT with a ViT-H/16 is able to outperform MAE-CT_{aug} on all benchmarks that use <1% of the labels. Furthermore, when strong augmentations are beneficial for low-shot finetuning (10% benchmark), MAE-CT can achieve competitive performances without *any* augmentations besides crop and flip at any point throughout training.

Clustering analysis. We assess the ability of MAE-CT to form object-specific clusters in two ways. First, we use the cluster accuracy [86, 83] to measure how well the ground truth classes of the validation set of ImageNet can be discovered using the unsupervised k -means clustering algorithm. The cluster accuracy ranges between 0 and 100, where 100 indicates a perfect match with the ground truth. Second, we calculate the silhouette score [69] to quantify the spread and compactness of the ground truth classes. The silhouette score ranges from -100 to 100, with 100 being the best value. Silhouette scores smaller than zero indicate that the clusters are not well separated.

Both cluster accuracy and silhouette score are reported in Table 3. Compared to MAE, MAE-CT shows a large improvement in cluster performance. The silhouette score

Architecture	Method	<i>low-shot evaluations</i>					<i>feature evaluations</i>	
		1 shot	2 shot	5 shot	1%	10%	Linear probing	k-NN
ViT-B/16	MAE [37]	14.0	27.1	43.1	54.2	73.4	68.0	51.1
	MoCo v3 [19]	37.4	47.7	57.3	63.4	74.7	76.7	72.6
	MSN [3]	50.3	58.9	65.5	69.5	75.5	77.7	76.3
	iBOT [91]	45.3	55.5	64.3	71.0	77.4	79.5	77.1
	Layer Grafting [51]	-	-	-	65.5	77.8	77.7	-
	MAE-CT	31.1	38.9	47.8	56.6	71.4*	73.5	64.1
	MAE-CT _{aug}	37.5	47.9	57.3	63.3	74.6	76.9	73.4
ViT-L/16	MAE [37]	14.3	34.9	56.9	67.7	79.3	76.0	60.6
	MSN [3]	47.5	55.5	62.5	67.0	71.4	77.3	76.2
	iBOT [91]	48.5	58.2	66.5	73.3	79.0	81.0	78.0
	Layer Grafting [51]	-	-	-	69.3	80.1	81.0	-
	MAE-CT	51.8	60.3	66.7	72.6	78.9*	80.2	78.0
	MAE-CT _{aug}	49.6	59.7	66.9	74.2	80.4	81.5	79.1
	MAE [37]	9.0	16.4	55.2	70.0	80.8	78.0	61.1
ViT-H/16	MAE-CT	53.1	62.3	68.9	75.0	80.4*	81.5	79.4
	MAE-CT _{aug}	50.1	60.2	67.7	75.0	81.0	82.2	79.8

Table 2. Low-shot and feature evaluations for different model sizes on ImageNet. "1 shot" means that, for each of the 1000 classes, a single label is available for training a classifier. "1%" is approximately "13 shot". MAE-CT_{aug} consistently improves low-shot and feature evaluation performance. As models get larger and fewer labels are used, MAE-CT is able to outperform methods that use extensive image augmentations with crop & flip only. * For 10% fine-tuning, extensive image augmentations are typically used, which we exclude for MAE-CT. Linear probing and k -NN evaluations are presented in the two rightmost columns.

improves from being negative, finding almost no cluster structure, to being positive showing separated clusters (see also Figure 1). For methods with extensive augmentation, MAE-CT_{aug} performs best for ViT-L/16, where we outperform iBOT even with MAE-CT. To the best of our knowledge, the cluster accuracy of MAE-CT (ViT-H/16) is state-of-the-art on ImageNet, when trained on ImageNet only. Further details are provided in Appendix B.3.

Method	B/16	L/16	H/16
<i>Minimal image augmentations</i>			
MAE	13.8 (-5.4)	14.3 (-4.1)	11.1 (-7.6)
MAE-CT	35.3 (1.1)	54.9 (11.0)	58.0 (8.4)
<i>Extensive image augmentations</i>			
MoCo v3 [18]	43.0 (4.5)	-	-
MSN [3]	54.2 (10.4)	45.4 (4.8)	-
iBOT [91]	50.0 (6.7)	52.0 (9.0)	-
MAE-CT _{aug}	46.2 (4.3)	56.9 (10.1)	54.8 (7.9)

Table 3. Comparison of k -means cluster accuracy on ImageNet. Parentheses show the silhouette score w.r.t. the ground truth.

4.4. Ablations and analysis

Ablation. We evaluate the impact of essential CT components in Table 4. Masking during contrastive tuning results in a moderate drop in performance, but enables training on a single GPU. The NNCLR head initialization, by training it on top of frozen encoder features before CT, is essential to

the performance gains. As MAE-CT does not use any augmentations besides crop and flip, the data-driven augmentation of the NN lookup is required to make the NNCLR task hard enough to learn a useful representation.

Method	Probing	k -NN
MAE-CT	80.2	77.4
apply masking (75%) during CT	79.4	75.3
skip NNCLR head initialization	78.5	68.1
NNCLR without NN lookup	70.6	40.5

Table 4. Ablation study for the essential CT components with ViT-L/16. Applying masking during CT or skipping the NNCLR head initialization on frozen encoder features results in a significant performance drop, especially in the k -NN accuracy. The NN-lookup is essential as only crop & flip are used as augmentations.

Computational cost. MAE-CT inherits the scalability of MAE as MAE pre-training takes up most of the training duration (shown in Table 5). Contrastive tuning is efficient as it is sufficient to train for a short duration. Additionally, the NNCLR loss is not backpropagated through the full encoder as we freeze half of the encoder blocks for contrastive tuning, which greatly reduces runtime and memory. By sacrificing a bit of performance (-0.8% in linear probing for ViT-L/16), contrastive tuning can also be applied with 75% masking of the input. This enables contrastive tuning on *all* considered model sizes on a *single* A100 80GB GPU where

even the larger models can be trained in roughly 1 day.

Method	B/16	L/16	H/16	H/14
<i>total GPU node-hours</i>				
MAE [37]	56	99	186	225
MAE-CT	2	5	15	19
MAE-CT _{aug}	6	9	18	24
<i>relative overhead over MAE</i>				
MAE-CT	3.7%	5.4%	7.9%	8.6%
MAE-CT _{aug}	10.9%	8.9%	9.9%	10.8%

Table 5. Required GPU node-hours of ViT models at different scales on a compute node with 8 NVIDIA A100 40GB GPUs. MAE-CT requires only a small amount of additional compute.

Effective invariance to data augmentation. We evaluate the average effective invariance [25] against rotations and different color augmentations. For an image x and its augmented version x_t , [25] defines the effective invariance (EI) as 0 if the linear classifier predicts different classes and $\sqrt{\hat{p}_t \cdot \hat{p}}$ if the predictions agree. \hat{p} denote the predictions for x and \hat{p}_t denote the predictions for x_t . Table 6 shows the average EI for rotations against 90°, 180° and 270° and for color augmentations that include changes in brightness, contrast, hue and saturation. We report the average EI for images in the validation set of ImageNet.

CT increases EI regarding rotations, where using extensive augmentations performs similar to not using them. The hand-crafted image augmentations used in MAE-CT_{aug} further increase the EI against color augmentations, but also MAE-CT improves over MAE. These results indicate that MAE-CT develops increased robustness against color transformations even though during training the color information in the input is not perturbed.

Method	B/16	L/16	H/16
<i>Effective invariance against rotations</i>			
MAE	0.288	0.413	0.450
MAE-CT	<u>0.433</u>	0.508	0.530
MAE-CT _{aug}	0.437	<u>0.505</u>	<u>0.529</u>
<i>Effective invariance against color augmentations</i>			
MAE	0.481	0.670	0.681
MAE-CT	<u>0.544</u>	<u>0.719</u>	<u>0.730</u>
MAE-CT _{aug}	0.714	0.783	0.786

Table 6. Effective Invariance (EI) against multiple transformations. MAE-CT increases the EI compared to MAE, showing that the NN lookup acts as a data-driven augmentation. MAE-CT_{aug} can further increase the EI against color augmentations due to the hand-crafted augmentations used during contrastive tuning.

4.5. Comparison to combined pre-training

Combined pre-training of MAE and NNCLR. In addition to the sequential MAE-CT approach, we also investigate the combined pre-training of MAE and NNCLR as depicted in the bottom left of Figure 2. To this end, we train a MAE with a ViT-L/16 encoder by additionally attaching a NNCLR head onto the [CLS] token of the encoder. During training we jointly optimize the MAE and NNCLR objectives where we balance the losses $\mathcal{L} = \mathcal{L}^{\text{MAE}} + \lambda \mathcal{L}^{\text{NNCLR}}$ with a λ of 0.001. Note, that we keep the augmentations from MAE, which are only cropping and flipping.

The upper half of Table 7 shows that the combined pre-training slightly improves over MAE but is far worse than MAE-CT. In addition to just combined pre-training, we investigate the application of CT after combined pre-training. We investigate different ways to initialize the NNCLR head before CT in the lower part of Table 7. For "combined pre-training + CT" we initialize a new NNCLR head by training it on top of frozen encoder features just like we do for MAE-CT. For "combined pre-training + CT_{skip}" we reuse the NNCLR head from combined pre-training directly for CT, which effectively *skips* the reinitialization of the NNCLR head. Additionally, instead of initializing an NNCLR head on top of the frozen encoder, one can train an NNCLR head during MAE training by inserting a stop gradient operation before the NNCLR head ("detached pre-training + CT_{skip}"). The results show that directly using the NNCLR head from pre-training for CT is slightly worse in addition to being more constrained as it requires modification of the MAE training process.

Overall the sequential approach of MAE-CT is more flexible, more efficient and achieves superior performances compared to the combined pre-training, even when CT is applied in addition to combined pre-training.

Method	Probing	k -NN
MAE	76.0	60.6
combined pre-training	77.8	66.1
combined pre-training + CT _{skip}	79.7	75.3
detached pre-training + CT _{skip}	80.1	77.0
combined pre-training + CT	80.1	76.7
MAE-CT	80.2	77.4

Table 7. Comparison of combined pre-training of MAE and NNCLR without and with applying CT. CT_{skip} reuses the head from combined pre-training directly for CT and "detached pre-training" adds a stop gradient operation before the NNCLR head during pre-training. All experiments use a ViT-L/16. Top: The combined pre-training slightly improves over MAE but is far worse than the sequential MAE-CT. Bottom: Reusing the NNCLR head from combined pre-training for CT ("CT_{skip}") can be a competitive alternative to initializing a new head on top of frozen encoder features, but is less flexible and overall slightly worse.

Shortcut learning of combined pre-training. In experiments with combined pre-training, we observe that even with a small choice of the NNCLR loss weight λ during combined pre-training, the NNCLR loss decreases immediately by about 30% compared to training a detached NNCLR head during combined pre-training. As the encoder does not have a good feature representation at the start of training, this indicates that the NNCLR head steers the encoder to extract basic features which drastically simplify the NNCLR objective. These basic features might be a symptom of shortcut learning.

Inspired by experiments conducted in [1] we evaluate to what degree the model preserves information about color statistics within the [CLS] token. We train a linear probe to predict the color histograms of the input image. In the combined pre-training, the NNCLR head pushes the encoder towards learning color statistic features (Figure 3), which is a form of shortcut learning as two views of the same image likely have a similar color histogram. These shortcut features evolve already in early encoder layers of the combined pre-training. While CT is able to partially correct them, they remain more dominant than in the sequentially trained encoder. Supervised fine-tuning of all layers — using hand-crafted image augmentations — can not fully mitigate this effect either. We describe the color histogram prediction task in more detail in Appendix A.4.

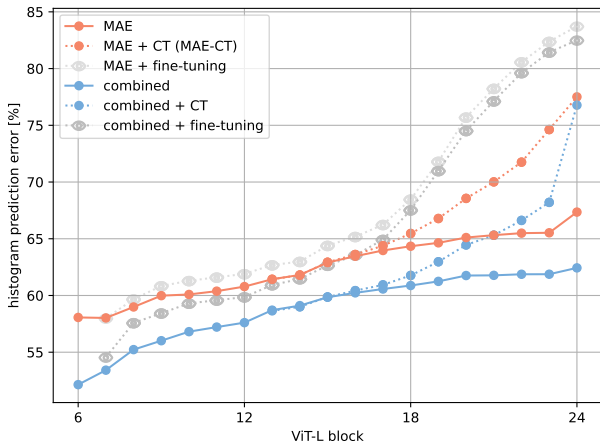


Figure 3. Measuring shortcut learning: Predicting the color histogram of input images from the [CLS] token after different blocks of a ViT-L (higher error is better). Combined pre-training learns shortcut features that can only partially be *forgotten* via CT or supervised fine-tuning. Sequential training avoids shortcut learning.

4.6. Clustering analysis

Cluster formation. To demonstrate the differences in clustering between tuning variants we provide results for ImageNet-Dogs15 [14], a subset of ImageNet commonly

utilized in the clustering literature. In Figure 4 we show the UMAP [60] embeddings of different MAE-CT (ViT-L) variations with their corresponding clustering accuracy. Here, combined pre-training performs slightly better than MAE. The UMAP embedding shows that except for the classes of *Norwegian Elkhound*, *Pug* and *Maltese Dog* none of the dog types are well separated. We suspect that these three dog breeds have only small intra-class variations in their characteristics, which makes them easily discernible by low level features. Once contrastive tuning is applied the cluster accuracy w.r.t. the 15 dog breeds improves by a factor of four and also the classes are visually better separated.

Cluster retrieval. In Figure 5 we show the nearest neighbors of two k -means cluster centroids for ImageNet-Dogs15 for MAE and MAE-CT (ViT-H/16). Inspecting the NNs of the cluster centroid indicates that MAE finds some clusters that correspond to image backgrounds, e.g. the first row contains dogs that are located inside and the second row contains dogs that are outside. This is also quantified by the low cluster accuracy w.r.t. the ground truth dog breeds of MAE. MAE reaches a cluster accuracy of 18.7% vs. 94.3% reached with MAE-CT. MAE-CT finds distinct clusters containing mostly images of a single class, shown by the perfect NN retrievals of dogs from the class *Basset* (third row) and *Norwegian Elkhound* (fourth row). Note, that the dogs are correctly grouped despite the different background. We provide the full retrieval, confusion matrices and UMAP embeddings in Appendix B.3.

5. Related Work

iBOT [91] and MSN [3] are state-of-the-art ID methods that successfully utilize masking of the student input. Both methods are more parameter efficient than MIM methods like MAE and perform excellent with ViT-B architectures, but they do not report a similar scaling ability as MAE-CT.

I-JEPA [4] is a recent work that overlaps with our goal to limit the use of hand-crafted, expert knowledge image augmentations. It achieves considerable speed-up due to a reduction in the number of costly encoder forward passes. Although I-JEPA does not generate views, it relies on a multi-block, non-overlapping masking strategy to create a prediction task for the student network. MAE-CT can apply random resized cropping, without such restrictions.

Layer Grafting [51] is recent work that combines MIM and ID pre-training in a sequential approach as well. Similar to our work, they want to preserve the MAE representation in lower layers and modify mainly the upper layers. Layer Grafting achieves this via a regularization loss applied to the lower third of the encoder, which requires an additional partial forward pass of the pre-trained MAE model. Furthermore, in Layer Grafting MAE pre-training is followed by the full training routine of MoCo v3. In

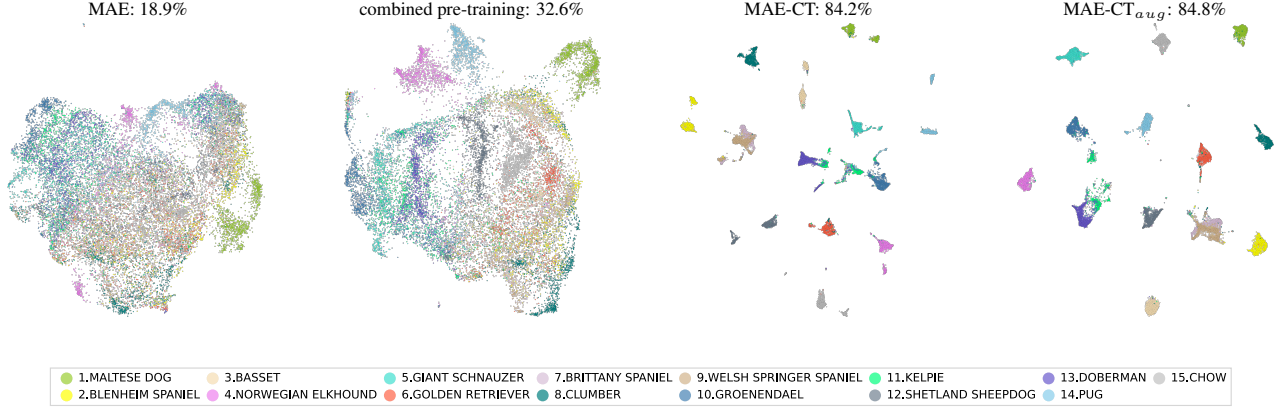


Figure 4. UMAP embeddings of MAE, combined pre-training, MAE-CT and MAE-CT_{aug} with corresponding k -means cluster accuracies for ImageNet-Dogs15. MAE-CT clearly improves the separation of the 15 classes. ViT-L/16 is used as encoder for all methods.

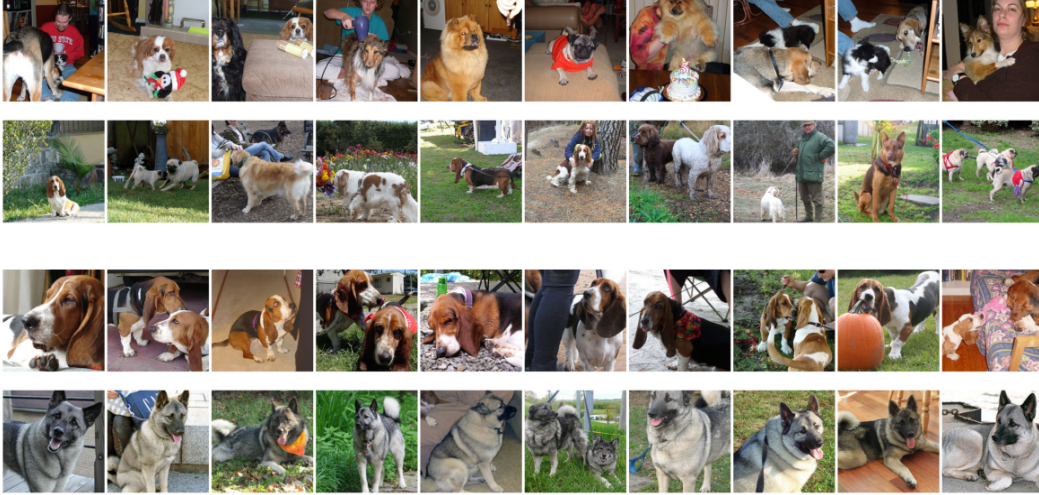


Figure 5. Ten NNs for two k -means cluster centers for MAE (upper) and MAE-CT (lower). Each row corresponds to one cluster found in the [CLS] token of ViT-H/16 for ImageNet-Dogs15. MAE groups the images into dogs located indoors (first row) and outdoors (second row) depending on the background. MAE-CT finds clusters that correspond to the specific dog breeds.

comparison, MAE-CT requires an order of magnitude less overhead due to the short duration of contrastive tuning.

6. Conclusion

We introduce MAE-CT, a self-supervised approach to combine the strengths of MIM and ID methods. We show that the NNCLR training objective — applied to an already pre-trained MAE model — is capable of creating object-specific clusters in its feature representation that come close to those of state-of-the-art ID methods. MAE-CT achieves this without labels or additional hand-crafted image augmentation. Given the strong dependence of ID methods on carefully selected image augmentations [75], this is a very promising result, which can be explained by the data-driven

augmentation effect of the NNCLR NN lookup when applied to features that already capture image semantics.

We show that our approach preserves the data efficiency of MAE. For larger ViT models, MAE-CT_{aug} — i.e. the version which applies standard augmentations in contrastive learning — outperforms previous methods trained on ImageNet in representation quality (linear probing, k -NN and cluster accuracy) as well as in low-shot classification.

Our work demonstrates the synergy between MIM and ID methods. MIM methods excel at the data efficient formation of highly useful lower level features, but provide less structured higher level features. ID methods, on the other hand, provide the ability to induce structure by learning object-focused, abstract representations without the need

for expensive annotations. MAE-CT successfully exploits the synergies between MIM and ID methods in a data efficient and flexible way, with little computational overhead.

Acknowledgements

The ELLIS Unit Linz, the LIT AI Lab, the Institute for Machine Learning, are supported by the Federal State Upper Austria. IARAI is supported by Here Technologies. We thank the projects AI-MOTION (LIT-2018-6-YOU-212), DeepFlood (LIT-2019-8-YOU-213), Medical Cognitive Computing Center (MC3), INCONTROL-RL (FFG-881064), PRIMAL (FFG-873979), S3AI (FFG-872172), DL for GranularFlow (FFG-871302), EPILEPSIA (FFG-892171), AIRI FG 9-N (FWF-36284, FWF-36235), ELISE (H2020-ICT-2019-3 ID: 951847), Stars4Waters (HORIZON-CL6-2021-CLIMATE-01-01). We thank Audi.JKU Deep Learning Center, TGW LOGISTICS GROUP GMBH, Silicon Austria Labs (SAL), FILL Gesellschaft mbH, Anyline GmbH, Google, ZF Friedrichshafen AG, Robert Bosch GmbH, UCB Biopharma SRL, Merck Healthcare KGaA, Verbund AG, GLS (Univ. Waterloo) Software Competence Center Hagenberg GmbH, TÜV Austria, Frauscher Sensonic and the NVIDIA Corporation

We thank the European High Performance Computing initiative for providing the computational resources that enabled this work. EHPC-DEV-2022D09-012, EHPC-DEV-2022D09-024, EHPC-DEV-2022D06-166, EHPC-DEV-2022D06-177, EHPC-DEV-2022D06-173

References

- [1] Sravanti Addepalli, Kaushal Bhogale, Priyam Dey, and R. Venkatesh Babu. Towards efficient and effective self-supervised learning of visual representations. In *ECCV (31)*, volume 13691 of *Lecture Notes in Computer Science*, pages 523–538. Springer, 2022. [8](#)
- [2] Mahmoud Assran, Randall Balestriero, Quentin Duval, Florian Bordes, Ishan Misra, Piotr Bojanowski, Pascal Vincent, Michael G. Rabbat, and Nicolas Ballas. The hidden uniform cluster prior in self-supervised learning. *CoRR*, abs/2210.07277, 2022. [3](#)
- [3] Mahmoud Assran, Mathilde Caron, Ishan Misra, Piotr Bojanowski, Florian Bordes, Pascal Vincent, Armand Joulin, Mike Rabbat, and Nicolas Ballas. Masked siamese networks for label-efficient learning. In *ECCV (31)*, volume 13691 of *Lecture Notes in Computer Science*, pages 456–473. Springer, 2022. [2](#), [5](#), [6](#), [8](#), [17](#), [21](#), [23](#)
- [4] Mahmoud Assran, Quentin Duval, Ishan Misra, Piotr Bojanowski, Pascal Vincent, Michael G. Rabbat, Yann LeCun, and Nicolas Ballas. Self-supervised learning from images with a joint-embedding predictive architecture. *arXiv preprint arXiv:2301.08243*, 2023. [5](#), [8](#), [17](#), [19](#), [21](#)
- [5] Lei Jimmy Ba, Jamie Ryan Kiros, and Geoffrey E. Hinton. Layer normalization. *CoRR*, abs/1607.06450, 2016. [15](#)
- [6] Alexei Baevski, Wei-Ning Hsu, Qiantong Xu, Arun Babu, Jiatao Gu, and Michael Auli. data2vec: A general framework for self-supervised learning in speech, vision and language. In *ICML*, volume 162 of *Proceedings of Machine Learning Research*, pages 1298–1312. PMLR, 2022. [1](#), [2](#), [3](#)
- [7] Hangbo Bao, Li Dong, Songhao Piao, and Furu Wei. Beit: BERT pre-training of image transformers. In *ICLR*. OpenReview.net, 2022. [1](#), [2](#)
- [8] Adrien Bardes, Jean Ponce, and Yann LeCun. Vi-creg: Variance-invariance-covariance regularization for self-supervised learning. In *ICLR*. OpenReview.net, 2022. [1](#), [2](#)
- [9] Zhaowei Cai, Avinash Ravichandran, Paolo Favaro, Manchen Wang, Davide Modolo, Rahul Bhotika, Zhuowen Tu, and Stefano Soatto. Semi-supervised vision transformers at scale. 08 2022. [17](#)
- [10] Mathilde Caron, Piotr Bojanowski, Armand Joulin, and Matthijs Douze. Deep clustering for unsupervised learning of visual features. In *ECCV (14)*, volume 11218 of *Lecture Notes in Computer Science*, pages 139–156, 2018. [2](#)
- [11] Mathilde Caron, Ishan Misra, Julien Mairal, Priya Goyal, Piotr Bojanowski, and Armand Joulin. Unsupervised learning of visual features by contrasting cluster assignments. 2020. [2](#)
- [12] Mathilde Caron, Ishan Misra, Julien Mairal, Priya Goyal, Piotr Bojanowski, and Armand Joulin. Unsupervised learning of visual features by contrasting cluster assignments. In *NeurIPS*, 2020. [5](#)
- [13] Mathilde Caron, Hugo Touvron, Ishan Misra, Hervé Jégou, Julien Mairal, Piotr Bojanowski, and Armand Joulin. Emerging properties in self-supervised vision transformers. In *ICCV*, pages 9630–9640. IEEE, 2021. [1](#), [2](#), [5](#), [16](#), [17](#), [18](#), [21](#), [23](#)
- [14] Jianlong Chang, Lingfeng Wang, Gaofeng Meng, Shiming Xiang, and Chunhong Pan. Deep adaptive image clustering. In *ICCV*, pages 5880–5888. IEEE Computer Society, 2017. [8](#), [22](#)
- [15] Mark Chen, Alec Radford, Rewon Child, Jeffrey Wu, Heewoo Jun, David Luan, and Ilya Sutskever. Generative pre-training from pixels. In *ICML*, volume 119 of *Proceedings of Machine Learning Research*, pages 1691–1703. PMLR, 2020. [2](#)
- [16] Mayee F. Chen, Daniel Y. Fu, Avaniika Narayan, Michael Zhang, Zhao Song, Kayvon Fatahalian, and Christopher Ré. Perfectly balanced: Improving transfer and robustness of supervised contrastive learning. In *ICML*, volume 162 of *Proceedings of Machine Learning Research*, pages 3090–3122. PMLR, 2022. [3](#)
- [17] Ting Chen, Simon Kornblith, Mohammad Norouzi, and Geoffrey E. Hinton. A simple framework for contrastive learning of visual representations. In *ICML*, volume 119 of *Proceedings of Machine Learning Research*, pages 1597–1607. PMLR, 2020. [1](#), [2](#), [3](#)
- [18] Xinlei Chen and Kaiming He. Exploring simple siamese representation learning. In *CVPR*, pages 15750–15758. Computer Vision Foundation / IEEE, 2021. [2](#), [6](#), [21](#), [23](#)
- [19] Xinlei Chen, Saining Xie, and Kaiming He. An empirical study of training self-supervised vision transformers. In *ICCV*, pages 9620–9629. IEEE, 2021. [5](#), [6](#), [17](#)
- [20] Kevin Clark, Minh-Thang Luong, Quoc V. Le, and Christopher D. Manning. ELECTRA: pre-training text encoders

- as discriminators rather than generators. In *ICLR*. OpenReview.net, 2020. 2, 5, 16, 17
- [21] David Frederic Crouse. On implementing 2d rectangular assignment algorithms. *IEEE Trans. Aerosp. Electron. Syst.*, 52(4):1679–1696, 2016. 22
- [22] Ekin Dogus Cubuk, Barret Zoph, Jonathon Shlens, and Quoc Le. Randaugment: Practical automated data augmentation with a reduced search space. In *NeurIPS*, 2020. 2, 17, 18
- [23] Tri Dao, Daniel Y. Fu, Stefano Ermon, Atri Rudra, and Christopher Ré. FlashAttention: Fast and memory-efficient exact attention with IO-awareness. In *NeurIPS*, 2022. 15
- [24] Jia Deng, Wei Dong, Richard Socher, Li-Jia Li, Kai Li, and Li Fei-Fei. Imagenet: A large-scale hierarchical image database. In *CVPR*, pages 248–255. IEEE Computer Society, 2009. 5
- [25] Weijian Deng, Stephen Gould, and Liang Zheng. On the strong correlation between model invariance and generalization. *arXiv preprint arXiv:2207.07065*, 2022. 7
- [26] Jacob Devlin, Ming-Wei Chang, Kenton Lee, and Kristina Toutanova. BERT: pre-training of deep bidirectional transformers for language understanding. In *NAACL-HLT (1)*, pages 4171–4186. Association for Computational Linguistics, 2019. 2, 18
- [27] Carl Doersch, Abhinav Gupta, and Alexei A. Efros. Unsupervised visual representation learning by context prediction. In *CVPR*, 2015. 2, 17
- [28] Alexey Dosovitskiy, Lucas Beyer, Alexander Kolesnikov, Dirk Weissenborn, Xiaohua Zhai, Thomas Unterthiner, Mostafa Dehghani, Matthias Minderer, Georg Heigold, Sylvain Gelly, Jakob Uszkoreit, and Neil Houlsby. An image is worth 16x16 words: Transformers for image recognition at scale. In *ICLR*. OpenReview.net, 2021. 2, 15
- [29] Debidatta Dwibedi, Yusuf Aytar, Jonathan Tompson, Pierre Sermanet, and Andrew Zisserman. With a little help from my friends: Nearest-neighbor contrastive learning of visual representations. In *ICCV*, pages 9568–9577. IEEE, 2021. 1, 2, 3, 4, 5, 15, 21
- [30] Alaaeldin El-Nouby, Gautier Izacard, Hugo Touvron, Ivan Laptev, Hervé Jégou, and Edouard Grave. Are large-scale datasets necessary for self-supervised pre-training? *arXiv preprint arXiv:2112.10740*, 2021. 2
- [31] Baruch Epstein and Ron Meir. Generalization bounds for unsupervised and semi-supervised learning with autoencoders. *CoRR*, abs/1902.01449, 2019. 3
- [32] Christoph Feichtenhofer, Haoqi Fan, Yanghao Li, and Kaiming He. Masked autoencoders as spatiotemporal learners. 2022. 3
- [33] Robert Geirhos, Jörn-Henrik Jacobsen, Claudio Michaelis, Richard S. Zemel, Wieland Brendel, Matthias Bethge, and Felix A. Wichmann. Shortcut learning in deep neural networks. *Nature Machine Intelligence*, 2(11):665–673, 2020. 2, 3
- [34] Priya Goyal, Piotr Dollár, Ross B. Girshick, Pieter Noordhuis, Lukasz Wesolowski, Aapo Kyrola, Andrew Tulloch, Yangqing Jia, and Kaiming He. Accurate, large minibatch SGD: training imagenet in 1 hour, 2017. 15, 17
- [35] Jean-Bastien Grill, Florian Strub, Florent Altché, Corentin Tallec, Pierre H. Richemond, Elena Buchatskaya, Carl Doersch, Bernardo Ávila Pires, Zhaohan Guo, Mohammad Gheshlaghi Azar, Bilal Piot, Koray Kavukcuoglu, Rémi Munos, and Michal Valko. Bootstrap your own latent - A new approach to self-supervised learning. In *NeurIPS*, 2020. 1, 2, 3, 5
- [36] Jeff Z. HaoChen and Tengyu Ma. A theoretical study of inductive biases in contrastive learning. *CoRR*, abs/2211.14699, 2022. 3
- [37] Kaiming He, Xinlei Chen, Saining Xie, Yanghao Li, Piotr Dollár, and Ross B. Girshick. Masked autoencoders are scalable vision learners. In *CVPR*, pages 15979–15988. IEEE, 2022. 1, 2, 3, 4, 5, 6, 7, 15, 17, 18, 19, 21
- [38] Kaiming He, Haoqi Fan, Yuxin Wu, Saining Xie, and Ross B. Girshick. Momentum contrast for unsupervised visual representation learning. In *CVPR*, pages 9726–9735. Computer Vision Foundation / IEEE, 2020. 1, 2, 3, 15
- [39] Kaiming He, Xiangyu Zhang, Shaoqing Ren, and Jian Sun. Deep residual learning for image recognition. In *CVPR*, pages 770–778. IEEE Computer Society, 2016. 3
- [40] Kaiming He, Xiangyu Zhang, Shaoqing Ren, and Jian Sun. Deep residual learning for image recognition. In *CVPR*, pages 770–778. IEEE Computer Society, 2016. 15
- [41] Dan Hendrycks, Steven Basart, Norman Mu, Saurav Kadavath, Frank Wang, Evan Dorundo, Rahul Desai, Tyler Zhu, Samyak Parajuli, Mike Guo, Dawn Song, Jacob Steinhardt, and Justin Gilmer. The many faces of robustness: A critical analysis of out-of-distribution generalization. In *ICCV*, pages 8320–8329. IEEE, 2021. 20
- [42] Dan Hendrycks, Kevin Zhao, Steven Basart, Jacob Steinhardt, and Dawn Song. Natural adversarial examples. *CVPR*, 2021. 20
- [43] R. Devon Hjelm, Alex Fedorov, Samuel Lavoie-Marchildon, Karan Grewal, Philip Bachman, Adam Trischler, and Yoshua Bengio. Learning deep representations by mutual information estimation and maximization. In *ICLR*. OpenReview.net, 2019. 2
- [44] Ronghang Hu, Shoubhik Debnath, Saining Xie, and Xinlei Chen. Exploring long-sequence masked autoencoders. *CoRR*, abs/2210.07224, 2022. 3, 19
- [45] Gao Huang, Yu Sun, Zhuang Liu, Daniel Sedra, and Kilian Q. Weinberger. Deep networks with stochastic depth. In *ECCV (4)*, volume 9908 of *Lecture Notes in Computer Science*, pages 646–661. Springer, 2016. 2, 17
- [46] Po-Yao Huang, Hu Xu, Juncheng Li, Alexei Baevski, Michael Auli, Wojciech Galuba, Florian Metze, and Christoph Feichtenhofer. Masked autoencoders that listen. *CoRR*, abs/2207.06405, 2022. 2, 3
- [47] Zhicheng Huang, Xiaojie Jin, Chengze Lu, Qibin Hou, Ming-Ming Cheng, Dongmei Fu, Xiaohui Shen, and Jiashi Feng. Contrastive masked autoencoders are stronger vision learners. *arXiv preprint arXiv:2207.13532*, 2022. 21
- [48] Lawrence Hubert and Phipps Arabie. Comparing partitions. *Journal of classification*, 2(1):193–218, 1985. 22
- [49] Sergey Ioffe and Christian Szegedy. Batch normalization: Accelerating deep network training by reducing internal co-

- variate shift. In *ICML*, pages 448–456. PMLR, 2015. 15, 17
- [50] Xu Ji, Andrea Vedaldi, and João F. Henriques. Invariant information clustering for unsupervised image classification and segmentation. In *ICCV*, pages 9864–9873. IEEE, 2019. 2
- [51] Ziyu Jiang, Yinpeng Chen, Mengchen Liu, Dongdong Chen, Xiyang Dai, Lu Yuan, Zicheng Liu, and Zhangyang Wang. Layer grafted pre-training: Bridging contrastive learning and masked image modeling for label-efficient representations. *CoRR*, abs/2302.14138, 2023. 5, 6, 8, 21
- [52] Dhiraj D. Kalamkar, Dheevatsa Mudigere, Naveen Mellem-pudi, Dipankar Das, Kunal Banerjee, Sasikanth Avancha, Dharma Teja Vooturi, Nataraj Jammalamadaka, Jianyu Huang, Hector Yuen, Jiyan Yang, Jongsoo Park, Alexander Heinecke, Evangelos Georganas, Sudarshan Srinivasan, Abhisek Kundu, Misha Smelyanskiy, Bharat Kaul, and Pradeep Dubey. A study of BFLOAT16 for deep learning training. *CoRR*, abs/1905.12322, 2019. 15
- [53] Khaled Koutini, Jan Schlüter, Hamid Eghbal-zadeh, and Gerhard Widmer. Efficient training of audio transformers with patchout. In *INTERSPEECH*, pages 2753–2757. ISCA, 2022. 2
- [54] Yunfan Li, Peng Hu, Zitao Liu, Dezhong Peng, Joey Tianyi Zhou, and Xi Peng. Contrastive clustering. *Proceedings of the AAAI Conference on Artificial Intelligence*, 35(10):8547–8555, 2021. 2
- [55] Yanghao Li, Saining Xie, Xinlei Chen, Piotr Dollár, Kaiming He, and Ross B. Girshick. Benchmarking detection transfer learning with vision transformers. *CoRR*, abs/2111.11429, 2021. 3
- [56] Stuart P. Lloyd. Least squares quantization in PCM. *IEEE Trans. Inf. Theory*, 28(2):129–136, 1982. 3
- [57] Ilya Loshchilov and Frank Hutter. Decoupled weight decay regularization. In *ICLR*, 2019. 16
- [58] James B. MacQueen. Some methods for classification and analysis of multivariate observations. In *Proc. 5th Berkeley Symposium on Math., Stat., and Prob.*, page 281, 1965. 3
- [59] Julien Mairal. Cyanure: An open-source toolbox for empirical risk minimization for python, c++, and soon more. *CoRR*, abs/1912.08165, 2019. 17
- [60] Leland McInnes, John Healy, Nathaniel Saul, and Lukas Großberger. UMAP: uniform manifold approximation and projection. *J. Open Source Softw.*, 3(29):861, 2018. 2, 8, 22
- [61] Lukas Miklautz, Lena G. M. Bauer, Dominik Mautz, Sebastian Tschiatschek, Christian Böhm, and Claudia Plant. Details (don’t) matter: Isolating cluster information in deep embedded spaces. In *IJCAI*, pages 2826–2832. ijcai.org, 2021. 3
- [62] Ishan Misra and Laurens van der Maaten. Self-supervised learning of pretext-invariant representations. In *CVPR*, pages 6706–6716. Computer Vision Foundation / IEEE, 2020. 1, 2
- [63] Xuan Vinh Nguyen, Julien Epps, and James Bailey. Information theoretic measures for clusterings comparison: Variants, properties, normalization and correction for chance. *J. Mach. Learn. Res.*, 11:2837–2854, 2010. 22
- [64] Advait Parulekar, Liam Collins, Karthikeyan Shanmugam, Aryan Mokhtari, and Sanjay Shakkottai. Infonce loss provably learns cluster-preserving representations. *CoRR*, abs/2302.07920, 2023. 3
- [65] Deepak Pathak, Philipp Krähenbühl, Jeff Donahue, Trevor Darrell, and Alexei A. Efros. Context encoders: Feature learning by inpainting. In *CVPR*, pages 2536–2544. IEEE Computer Society, 2016. 2
- [66] F. Pedregosa, G. Varoquaux, A. Gramfort, V. Michel, B. Thirion, O. Grisel, M. Blondel, P. Prettenhofer, R. Weiss, V. Dubourg, J. Vanderplas, A. Passos, D. Cournapeau, M. Brucher, M. Perrot, and E. Duchesnay. Scikit-learn: Machine learning in Python. *Journal of Machine Learning Research*, 12:2825–2830, 2011. 22
- [67] Maithra Raghu, Thomas Unterthiner, Simon Kornblith, Chiyuan Zhang, and Alexey Dosovitskiy. Do vision transformers see like convolutional neural networks? In *NeurIPS*, pages 12116–12128, 2021. 2
- [68] Benjamin Recht, Rebecca Roelofs, Ludwig Schmidt, and Vaishal Shankar. Do imagenet classifiers generalize to imagenet? In *ICML*, volume 97 of *Proceedings of Machine Learning Research*, pages 5389–5400. PMLR, 2019. 20
- [69] Peter J. Rousseeuw. Silhouettes: a graphical aid to the interpretation and validation of cluster analysis. *Journal of computational and applied mathematics*, 20:53–65, 1987. 5
- [70] Nikunj Saunshi, Orestis Plevrakis, Sanjeev Arora, Mikhail Khodak, and Hrishikesh Khandeparkar. A theoretical analysis of contrastive unsupervised representation learning. In *ICML*, volume 97 of *Proceedings of Machine Learning Research*, pages 5628–5637. PMLR, 2019. 3
- [71] D. Sculley. Web-scale k-means clustering. In *WWW*, pages 1177–1178. ACM, 2010. 22
- [72] Mannat Singh, Quentin Duval, Kalyan Vasudev Alwala, Haoqi Fan, Vaibhav Aggarwal, Aaron Adcock, Armand Joulin, Piotr Dollár, Christoph Feichtenhofer, Ross B. Girshick, Rohit Girdhar, and Ishan Misra. The effectiveness of MAE pre-pretraining for billion-scale pretraining. *arXiv preprint arXiv:2303.13496*, 2023. 3
- [73] Christian Szegedy, Vincent Vanhoucke, Sergey Ioffe, Jonathon Shlens, and Zbigniew Wojna. Rethinking the inception architecture for computer vision. In *CVPR*, pages 2818–2826. IEEE Computer Society, 2016. 16, 17, 18
- [74] Antti Tarvainen and Harri Valpola. Mean teachers are better role models: Weight-averaged consistency targets improve semi-supervised deep learning results. In *NIPS*, pages 1195–1204, 2017. 15
- [75] Yonglong Tian, Chen Sun, Ben Poole, Dilip Krishnan, Cordelia Schmid, and Phillip Isola. What makes for good views for contrastive learning? In *NeurIPS*, 2020. 2, 9
- [76] Zhan Tong, Yibing Song, Jue Wang, and Limin Wang. Videomae: Masked autoencoders are data-efficient learners for self-supervised video pre-training. 2022. 3
- [77] Ashish Vaswani, Noam Shazeer, Niki Parmar, Jakob Uszkoreit, Llion Jones, Aidan N. Gomez, Lukasz Kaiser, and Illia Polosukhin. Attention is all you need. In *NeurIPS*, pages 5998–6008, 2017. 15
- [78] Pascal Vincent, Hugo Larochelle, Yoshua Bengio, and Pierre-Antoine Manzagol. Extracting and composing robust

- features with denoising autoencoders. In *ICML*, volume 307 of *ACM International Conference Proceeding Series*, pages 1096–1103. ACM, 2008. [3](#)
- [79] Feng Wang and Huaping Liu. Understanding the behaviour of contrastive loss. In *CVPR*, pages 2495–2504. Computer Vision Foundation / IEEE, 2021. [16](#)
- [80] Haohan Wang, Songwei Ge, Zachary C. Lipton, and Eric P. Xing. Learning robust global representations by penalizing local predictive power. In *NeurIPS*, pages 10506–10518, 2019. [20](#)
- [81] Tongzhou Wang and Phillip Isola. Understanding contrastive representation learning through alignment and uniformity on the hypersphere. In *ICML*, volume 119 of *Proceedings of Machine Learning Research*, pages 9929–9939. PMLR, 2020. [16](#)
- [82] Zhirong Wu, Yuanjun Xiong, Stella X. Yu, and Dahua Lin. Unsupervised feature learning via non-parametric instance discrimination. In *CVPR*, pages 3733–3742. Computer Vision Foundation / IEEE Computer Society, 2018. [17](#)
- [83] Junyuan Xie, Ross B. Girshick, and Ali Farhadi. Unsupervised deep embedding for clustering analysis. In *ICML*, volume 48 of *JMLR Workshop and Conference Proceedings*, pages 478–487. JMLR.org, 2016. [2, 3, 5](#)
- [84] Zhenda Xie, Zheng Zhang, Yue Cao, Yutong Lin, Jianmin Bao, Zhuliang Yao, Qi Dai, and Han Hu. Simmim: a simple framework for masked image modeling. In *CVPR*, pages 9643–9653. IEEE, 2022. [1, 2, 3, 5, 21](#)
- [85] Bo Yang, Xiao Fu, Nicholas D. Sidiropoulos, and Mingyi Hong. Towards k-means-friendly spaces: Simultaneous deep learning and clustering. In *ICML*, volume 70 of *Proceedings of Machine Learning Research*, pages 3861–3870. PMLR, 2017. [3](#)
- [86] Yi Yang, Dong Xu, Feiping Nie, Shuicheng Yan, and Yuet-ing Zhuang. Image clustering using local discriminant models and global integration. *IEEE Trans. Image Process.*, 19(10):2761–2773, 2010. [5, 22](#)
- [87] Sangdoo Yun, Dongyoon Han, Sanghyuk Chun, Seong Joon Oh, Youngjoon Yoo, and Junsuk Choe. Cutmix: Regularization strategy to train strong classifiers with localizable features. In *ICCV*, pages 6022–6031. IEEE, 2019. [2, 17, 18](#)
- [88] Jure Zbontar, Li Jing, Ishan Misra, Yann LeCun, and Stéphane Deny. Barlow twins: Self-supervised learning via redundancy reduction. In *ICML*, volume 139 of *Proceedings of Machine Learning Research*, pages 12310–12320. PMLR, 2021. [1, 2, 3, 5](#)
- [89] Hongyi Zhang, Moustapha Cissé, Yann N. Dauphin, and David Lopez-Paz. mixup: Beyond empirical risk minimization. In *ICLR*. OpenReview.net, 2018. [2, 17, 18](#)
- [90] Zhun Zhong, Liang Zheng, Guoliang Kang, Shaozi Li, and Yi Yang. Random erasing data augmentation. In *AAAI*, pages 13001–13008. AAAI Press, 2020. [17, 18](#)
- [91] Jinghao Zhou, Chen Wei, Huiyu Wang, Wei Shen, Cihang Xie, Alan L. Yuille, and Tao Kong. Image BERT pre-training with online tokenizer. In *ICLR*. OpenReview.net, 2022. [2, 5, 6, 8, 17, 21, 23](#)
- [92] Sheng Zhou, Hongjia Xu, Zhuonan Zheng, Jiawei Chen, Zhao Li, Jiajun Bu, Jia Wu, Xin Wang, Wenwu Zhu, and Martin Ester. A comprehensive survey on deep clustering: Taxonomy, challenges, and future directions. *CoRR*, abs/2206.07579, 2022. [2, 3](#)

Appendix

A. Reproducibility

A.1. Implementation details

General All experiments use the linear lr scaling rule [34] $lr = base\ lr \times batch\ size \times views / 256$ where $views = 2$ for CT and $views = 1$ otherwise. Bias and normalization parameters (weights of LayerNorm and BatchNorm layers) are excluded from the weight decay.

In experiments with float16 we frequently encountered overflows in the attention matrix leading to inf activations, therefore we train all our models in bfloat16 [52] precision. We use FlashAttention [23], which speeds up training by approximately 40/30/20% for ViT-B/L/H respectively.

MAE reimplementation. In early experiments, we investigated combined pre-training of MAE and NNCLR with a stop gradient operation between encoder and NNCLR head. This effectively corresponds to normal MAE pre-training as the NNCLR head *does not* influence the MAE pre-training. The only difference is that two views (generated with the augmentations used for MAE pre-training) are used. To account for this difference, we reduce the number of pre-training epochs from 1600 to 800. Additionally, we train with a lower batch size due to memory constraints (1024 for ViT-B/L and 512 for ViT-H). We train a ViT-B/16, ViT-L/16 and ViT-H/16 using this procedure, which we use throughout the main paper. For ViT-H/14 we use the publicly available checkpoint. Table 8 shows that the performance of our re-implementation is nearly identical to the original.

Method	Probing	k-NN
MAE _{public}	75.8	60.6
MAE _{reimpl}	75.9	57.6
MAE _{public} -CT	80.2	77.3
MAE _{reimpl} -CT	80.2	77.4

Table 8. Validation of our MAE re-implementation by comparing to the original publicly released checkpoint of a ViT-L/16.

Required GPU hours benchmark. Figure 6 shows the required GPU hours benchmarked on a node with 4 NVIDIA A100 40GB GPUs using bfloat16 precision and FlashAttention [23]. A batch size of 2048/1024/512 is used for ViT-B/L/H respectively, which is the maximal possible batch size for MAE training on 4xA100 40GB. MAE-CT uses the default setting of freezing half of the ViT blocks and can only fit half of the MAE batch size. Total GPU hours are extrapolated from a short benchmark run.

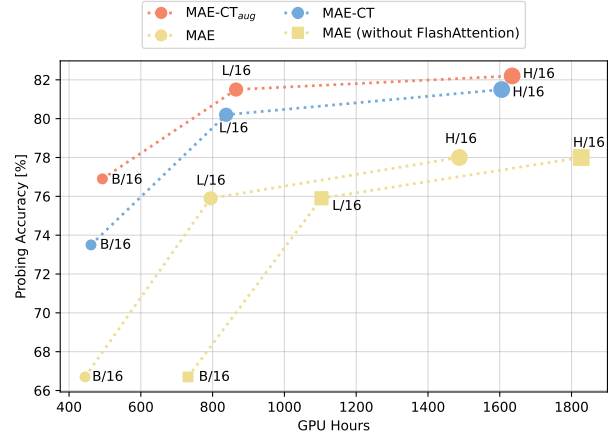


Figure 6. GPU-hours vs linear probing accuracy. MAE-CT is able to form abstract representations with little overhead. The impact of hand-crafted augmentations decreases as model size increases.

A.2. Contrastive tuning

ViT architecture. We follow MAE [37] and use the standard ViT architecture [28]. The ViT projects the input images into patch tokens with a non-overlapping convolutional layer (stride = kernel size), adds a fixed 2D sine-cosine positional embedding [77] to each patch token, appends an auxiliary [CLS] token and then processes all tokens with a stack of transformer blocks. A transformer block consists of two modules, namely a multi-head self-attention and a 2-layer MLP, which are applied sequentially. Both modules are preceded by a LayerNorm [5] layer and are wrapped with a residual connection [40]. After the last transformer block, a final LayerNorm is applied. We use the [CLS] token of the encoder output as input to the NNCLR head and all evaluations. For ViT-B/16, we use the average of the patch tokens instead of the [CLS] token.

NNCLR architecture. We follow the design of the original NNCLR head [29] and use a 3-layer MLP as projector and a 2-layer MLP as predictor. Each MLP layer is followed by a BatchNorm [49] except the last predictor layer. Each BatchNorm layer is followed by a ReLU activation except the last projector layer. BatchNorm statistics are calculated per view. To stabilize the entries written into the queue, we apply a fast moving exponential moving average (EMA) [38, 74] to the projector MLP in the topk-NN lookup path.

NNCLR initialization Before contrastive tuning, we train an NNCLR head with the encoder fully frozen to adjust the NNCLR head to the encoder features using top1-NN lookup, a learning rate of $1e - 4$, no EMA in the projector, a temperature τ of 0.15 and a training duration of 20 epochs

for all model sizes and variants. Other hyperparameters follow the ones from contrastive tuning (Table 9 and 10).

Contrastive tuning. Algorithm 1 describes the process of contrastive tuning in a PyTorch-like pseudo code. Table 9 and 10 list the hyperparameters used during contrastive tuning of MAE-CT and MAE-CT_{aug}, respectively. We find higher values for the temperature τ to perform best with ViT-H models. We argue that this is caused by the increased capacity of ViT-H and that a higher τ controls the alignment and uniformity trade-off [81] in the InfoNCE loss. Therefore, a higher τ slows down the expansion of clusters, as observed in [79]. It is common practice in student-teacher ID methods to use the teacher version of the encoder after training [13]. Thus, we use an exponential moving average (EMA) version of the encoder after contrastive tuning.

Algorithm 1 PyTorch-style pseudocode description of contrastive tuning using an adapted NNCLR head

```
# f: ViT encoder .. lower half of the encoder is frozen
# g: projector .. 3 layer MLP, hidden 2048, output 256
# h: predictor .. 2 layer MLP, hidden 4096, output 256
# Q: queue .. shift register of length 65536
# f_m: slow EMA of encoder f .. the model used after CT
# t1: 0.9999 .. momentum parameter of f_m
# g_m: fast EMA of projector g
# t2: 0.99 .. momentum parameter of g_m

# load a minibatch x
for x in loader:
    # two randomly augmented versions of x
    x1, x2 = augment(x), augment(x)
    # encoder forward passes
    y1, y2 = f(x1), f(x2)
    # predictor path for each y
    p1, p2 = h(g(y1)), h(g(y2))
    # NN path for each y
    z1, z2 = g_m(y1), g_m(y2)
    # L2-normalize embeddings
    p1, p2 = normalize(p1, dim=1), normalize(p2, dim=1)
    z1, z2 = normalize(z1, dim=1), normalize(z2, dim=1)
    # topk-NN lookup for each z
    nn1 = topk_NN(z1, Q, k)
    nn2 = topk_NN(z2, Q, k)
    # symmetrised InfoNCE loss
    loss = L(nn1, p2)/2 + L(nn2, p1)/2
    # optimization step
    loss.backward()
    optimizer.step()
    # shift embeddings z1 into queue Q
    update_queue(Q, z1)
    # EMA weight updates
    f_m = t1 * f_m + (1 - t1) * f
    g_m = t2 * g_m + (1 - t2) * g

# topk-NN lookup
def topk_NN(z, Q, k):
    similarities = z @ Q.T # matrix multiplication
    # calculate list of topk-NN
    candidates = similarities.topk(k, dim=1).indices
    # uniform sampling
    dice = torch.randint(size=(length(Q),), high=k)
    idx = candidates[torch.arange(length(Q)), dice]
    return Q[idx]

# InfoNCE loss
def L(nn, p, temperature=0.15):
    logits = nn @ p.T # matrix multiplication
    logits /= temperature # sharpening
    labels = torch.arange(p.shape[0])
    loss = cross_entropy(logits, labels)
    return loss
```

MAE-CT	Base	Large	Huge
Epochs	20	20	30
Batch size	1024	1024	512
Optimizer	AdamW [57]		
Momentum	$\beta_1 = 0.9, \beta_2 = 0.95$		
Learning rate schedule	warmup \rightarrow cosine		
Warmup fraction [73]	20 %	20 %	20 %
Encoder			
Learning rate	1e-4	1e-4	1e-4
Layer-wise lr decay [20]	0.65	0.65	0.65
Weight decay	0.05	0.05	0.05
Frozen layers	6	12	16
EMA	0.9999	0.9999	0.9999
NNCLR head			
Learning rate	1e-4	1e-4	1e-4
Weight decay	1e-5	1e-5	1e-5
Temperature τ	0.15	0.2	0.3
topk-NN k	20	20	20
Projector EMA	0.99	0.99	0.995

Table 9. MAE-CT hyperparameters.

MAE-CT _{aug}	Base	Large	Huge
Epochs	80	40	40
Batch size	1024	1024	512
Optimizer	AdamW [57]		
Momentum	$\beta_1 = 0.9, \beta_2 = 0.95$		
Learning rate schedule	warmup \rightarrow cosine		
Warmup fraction [73]	20 %	20 %	20 %
Encoder			
Learning rate	1e-4	1e-4	1e-4
Layer-wise lr decay [20]	0.65	0.65	0.65
Weight decay	0.05	0.05	0.05
Frozen layers	6	12	16
EMA	0.9999	0.9999	0.9999
NNCLR head			
Learning rate	5e-4	5e-4	5e-4
Weight decay	1e-5	1e-5	1e-5
Temperature τ	0.15	0.15	0.35
topk-NN k	10	10	30
Projector EMA	0.99	0.99	0.995

Table 10. MAE-CT_{aug} hyperparameters.

A.3. Evaluation

Linear probing. We follow common linear probing protocols and sweep over learning rates [91, 13, 4] and insert a non-affine BatchNorm [49] layer after the fully frozen encoder [27, 37, 3]. Adding a BatchNorm layer does *not* break the linearity property as it can be absorbed into the linear layer after training. Table 11 lists all parameters.

Config	Value
Epochs	50
Batch size	1024
Optimizer	SGD
Momentum	0.9
Weight decay	0
Learning rate	
Peak	{0.1, 0.09, ..., 0.01}
Schedule	warmup \rightarrow cosine
Warmup epochs [34]	5
Augmentations	
RandomResizedCrop	224 ²
RandomHorizontalFlip	$p = 0.5$

Table 11. Linear probing hyperparameters.

k -NN classification. We also evaluate the feature representation via a weighted k -NN classifier following the protocol in DINO [82, 13]. We sweep over different k for every compared method and find $k = 10$ to perform well for MAE-CT and MAE-CT_{aug}. For public checkpoints that do not report k -NN accuracies in their original publication, we report the best accuracy over different k for each checkpoint (which is also $k = 10$ most of the time). The weighted k -NN classifier takes the k training samples with the highest cosine similarity and weights each neighbors class by its cosine similarity with the test sample.

Low-shot classification. When using 10% of the ImageNet labels, we use the low-shot fine-tuning protocol of I-JEPA [4] to evaluate all compared ID methods (Table 12). We find that all MAE models and the huge models of MAE-CT_{aug} benefit from more regularization in this setting and therefore use the protocol from the original MAE publication [37], which uses Mixup [89], Cutmix [87], RandomErase [90], DropPath [45] in addition to RandAugment [22] as well as a higher learning rate ($1e - 3$).

In the 1% label regime, the protocols of related work vary between fine-tuning [4] and logistic regression [13]. Therefore, we explore logistic regression, the fine-tuning protocol used above and said protocol but with only crop & flip as input augmentations. We find MAE, MAE-CT and MAE-CT_{aug} to consistently perform better with only crop & flip and report the performance of the best protocol for competing methods. The best performing protocols

are: fine-tuning with only crop & flip for MAE, logistic regression for MoCo v3 [19], fine-tuning for iBOT [91] and logistic regression for MSN [3]. Following [9] we use a higher lr ($1e - 2$) for MAE with ViT-H.

For fine-tuning MAE-CT on 10% and 1% of the labels, we exclude *all* input augmentations besides crop & flip in all evaluation protocols, use a higher learning rate ($1e - 3$) and use the same DropPath [45] parameters as in the MAE fine-tuning protocol (0.1/0.2/0.3 for ViT-B/L/H).

For low-shot evaluations with 1, 2 or 5 labeled samples per class we train a L_2 -regularized logistic regression using the `cyanure` package [59] with hyperparameters from previous works [13, 3]. As MAE also benefits from fine-tuning in this low-data regime, we additionally explore full fine-tuning and fine-tuning the last encoder block where we find full fine-tuning to perform best overall. In extreme cases (1 and 2 labels per class with ViT-H) fine-tuning the last block and logistic regression perform slightly better, but we report the full fine-tuning results for consistency.

Config	Value
Epochs	100 (B), 50 (L/H)
Batch size	512
Optimizer	AdamW
Momentum	$\beta_1 = 0.9, \beta_2 = 0.999$
Weight decay	0.05
Learning rate	
Peak	3e-5
Schedule	warmup \rightarrow cosine
Warmup epochs [34]	5
Layer-wise lr decay [20]	0.65 (B), 0.75 (L/H)
DropPath [45]	0.0
Label smoothing [73]	0.1
Augmentations	
RandomResizedCrop	224 ²
RandomHorizontalFlip	$p = 0.5$
RandAugment [22]	
num_layers	2
magnitude	9

Table 12. Low-shot fine-tuning hyperparameters.

A.4. Analysis

Color histogram prediction. We evaluate the amount of information about color statistics by constructing a color histogram prediction task. We calculate the color histograms of an input image, discretize it into 64 bins and normalize it such that the sum of all bins of each color channel is equal to 1. This results in a total of 192 values which we regress with a L1 loss. To make the loss interpretable, we normalize it by dividing it by the average loss on the ImageNet validation set when predicting a uniform distribution (which evaluates to approximately 0.01204). We call the

average over these 192 normalized loss values "histogram prediction error", which can be interpreted as a percentage where 0% is achieved by perfectly predicting the histograms and 100% is the random performance.

We concurrently train 24 linear probes using the [CLS] tokens of each of the 24 ViT-L layers with a slightly modified version of the setting described in Table 11. We train for 10 epochs with 1 warmup epoch and a learning rate of 0.1. The encoder is fully frozen throughout training.

B. Experiments extended

B.1. Hyperparameter sensitivity study.

We evaluate the sensitivity of chosen hyperparameters on a ViT-L/16 in Table 13. MAE-CT works well across a range of hyperparameters.

Training epochs	10	20	30	-
Probing accuracy	79.57	80.23	80.24	-
k -NN accuracy	76.23	77.36	76.81	-
Trainable layers	6	12	15	18
Probing accuracy	79.76	80.23	80.26	80.12
k -NN accuracy	76.91	77.36	77.43	77.49
Encoder EMA	0.0	0.999	0.9999	-
Probing accuracy	80.19	80.21	80.23	-
k -NN accuracy	77.29	77.23	77.36	-
Temperature τ	0.15	0.2	0.25	-
Probing accuracy	80.12	80.23	80.12	-
k -NN accuracy	77.18	77.36	77.39	-
k -NN lookup k	1	10	20	30
Probing accuracy	80.23	80.16	80.17	80.29
k -NN accuracy	77.36	77.98	77.98	77.90
Projector EMA	0.0	0.99	0.995	0.999
Probing accuracy	80.07	80.23	80.16	80.13
k -NN accuracy	77.13	77.36	77.31	77.08

Table 13. Sensitivity analysis of MAE-CT with ViT-L/16. Default parameters used in this analysis are marked in gray.

B.2. Results & Ablations

Supervised MAE-CT. To explore the effect of perfect nearest neighbor retrieval, we apply contrastive tuning to a MAE pre-trained ViT-L/16 with an oracle (MAE-CT_{oracle}) where only samples of the same class are considered as candidates for the nearest neighbor lookup. After 30 epochs of contrastive tuning such a model achieves 83.9% linear probing performance. In Table 14 we compare it against a fully fine-tuned MAE with varying degrees of input augmentations. With only crop & flip augmentation, MAE-CT_{oracle} outperforms full fine-tuning.

We also validate our fine-tuning pipeline by fine-tuning our MAE pre-trained ViT-L/16 according to the fine-tuning

protocol of MAE [37]. We achieve a similar performance of 85.8% compared to 85.9% reported in MAE.

Method	Accuracy
<i>Crop & flip only</i>	
MAE-CT _{oracle} linear probe	83.9
MAE fine-tuned	83.1
+ Label smoothing [73]	83.7
<i>Additional input augmentations</i>	
+ Mixup [89]	84.5
+ Cutmix [87]	84.8
+ RandomErasing [90]	84.8
+ RandAugment [22]	85.8

Table 14. MAE-CT_{oracle} with linear probing compared to fine-tuning a MAE on ImageNet with a ViT-L/16 as encoder. When only crop & flip is used, MAE-CT_{oracle} performs better with linear probing than a fully fine-tuned MAE. Rows starting with "+" add an additional component to the setting of the previous row.

Representations for linear probing. Following previous works [13, 26], we evaluate the representation of the concatenation of the features from the last l ViT blocks as well as the concatenation of the [CLS] token with the average pooled patch tokens. Table 15 shows that $l = 6$ works well for our larger models while the concatenation of the [CLS] and the average of the patch tokens works best for ViT-B/16. We provide these results solely for the sake of completeness and to provide a point of reference. We do not apply this protocol when we compare to other methods.

concat l last layers		1	2	4	6	1 [†]
MAE-CT B/16		73.5	73.2	74.2	74	74.5
MAE-CT L/16		80.2	80.3	80.5	80.8	80.3
MAE-CT H/16		81.5	81.6	81.6	81.6	81.6
MAE-CT _{aug} B/16		76.9	75.5	76.0	75.9	77.5
MAE-CT _{aug} L/16		81.5	81.6	81.8	81.8	81.6
MAE-CT _{aug} H/16		82.2	82.2	82.4	82.3	82.3

Table 15. ImageNet linear probing performance when concatenating the features of the last l layers. [†]: concatenation of the [CLS] token and the average of all patch tokens of the last layer.

Fine-tuning with 100% of the labels. We visualize MAE-CT_{aug} against MAE and iBOT using various amounts of labels in Figure 7. Since CT aims to form abstractions that are useful when tiny amounts of labeled data is available, it is expected to *forget* about some details in the representation. These details can be leveraged when a sufficient amount of labels is available. However, MAE-CT_{aug} preserves most of these details and is able to outperform other ID methods on fine-tuning with 100% of the labels. MAE-CT_{aug} achieves 85.5 % fine-tuning accuracy.

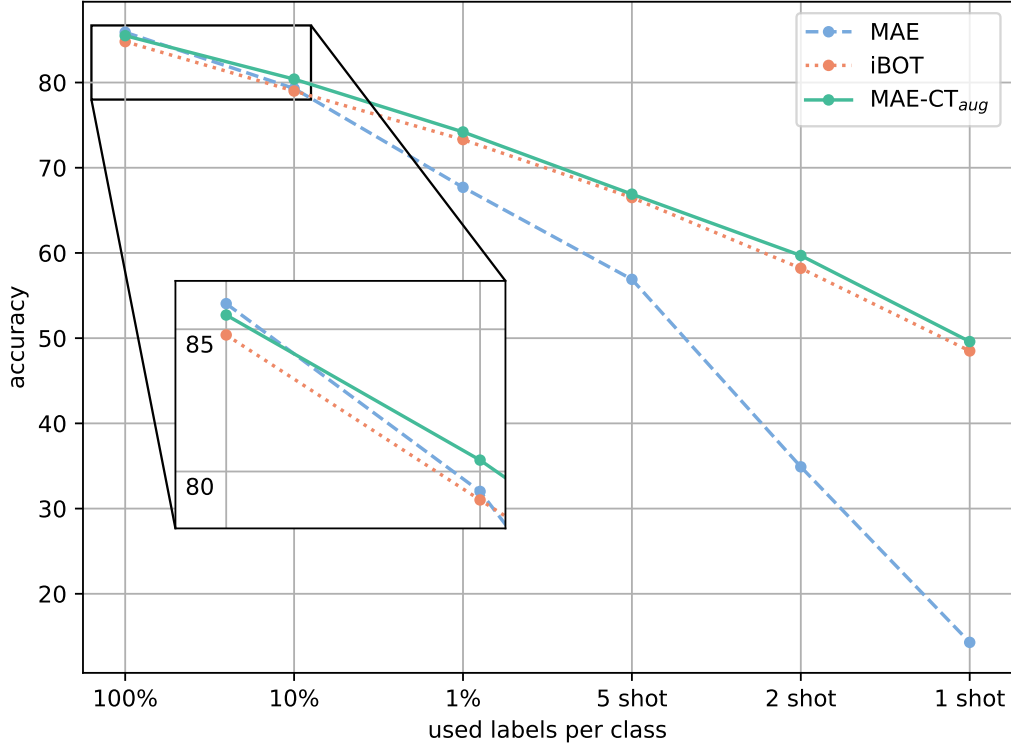


Figure 7. ImageNet fine-tuning accuracy using a ViT-L/16. MAE-CT_{aug} drastically increases low-shot performance at the cost of a slight decrease in performance when large amounts of labels are available. CT is beneficial starting from ~130K labels (10%).

Architecture	Method	low-shot evaluations					feature evaluations	
		1 shot	2 shot	5 shot	1%	10%	Linear probing	k-NN
ViT-H/16	MAE [37]	9.0	16.4	55.2	70.0	80.8	78.0	61.1
	MAE-CT	53.1	62.3	68.9	75.0	80.4*	81.5	79.4
	MAE-CT _{aug}	50.1	60.2	67.7	75.0	81.0	82.2	79.8
ViT-H/14	MAE [37]	7.2	14.1	40.2	72.8	81.2	77.2	58.9
	I-JEPA [4]	-	-	-	73.3	-	79.3	-
	MAE-CT	49.4	59.6	67.4	74.4	80.6*	81.3	79.1
	MAE-CT _{aug}	45.5	56.2	64.9	74.0	81.7	82.0	78.9

Table 16. Low-shot and feature evaluations of ViT-H models on ImageNet. The coupling of patch size with mask size of MAE degrades representation quality as analyzed by [44]. Given the inferior starting point of MAE H/14, MAE-CT is still able to leverage the longer sequence length when sufficiently many labels are available (10%), but falls short to the ViT-H/16 model otherwise.

*For 10% fine-tuning, extensive augmentations are typically used, which we exclude for MAE-CT.

Results with ViT-H/14. As analyzed by [44], MAE couples the patch size and the mask size since the mask is sampled on a per patch basis. A smaller patch size results in an easier reconstruction task as the average distance between visible patches is reduced. In experiments with ViT-H/14, we find that this coupling leads to a significant degrade in initial representation quality, which manifests in a 2.1% drop in k-NN accuracy and a 0.8% drop in linear probing accuracy (Table 16). Since MAE-CT uses the encoder of

a pre-trained MAE, it relies on a good encoder representation. While contrastive tuning can achieve similarly large performance gains on ViT-H/14 when compared to MAE, it only surpasses the ViT-H/16 results on the 10% low-shot benchmark where the number of labels is sufficient to benefit from the increased sequence length. Despite this special interaction in the MAE pre-training, MAE-CT is still able to surpass competing methods using the ViT-H/14 model.

Robustness and transfer. We evaluate the linear probe trained on ImageNet on four transfer learning datasets. Namely, ImageNet-V2 [68], ImageNet-R [41], ImageNet-Sketch [80] and ImageNet-A [42]. In Table 17 we compare the top-1 accuracy of ViT-L/16 models. The results show a small, but overall consistent benefit of the stronger augmentation effect provided by higher values of k in the topk-NN lookup for MAE-CT. MAE-CT_{aug} is more robust to distribution shift, which is expected, given that the hand-crafted image augmentations are designed to induce color invariance, while MAE-CT still utilizes color information to cluster samples. The gap between MAE-CT and MAE-CT_{aug} becomes larger with increase in distribution shift of the datasets (from left to right), but always improves MAE.

Method	k	V2	R	Sketch	A
MAE	-	71.7	37.0	24.3	12.3
MAE-CT	1	76.4	41.2	27.6	20.5
MAE-CT	10	<u>76.6</u>	42.0	28.2	20.8
MAE-CT	20	76.5	<u>42.2</u>	28.1	21.4
MAE-CT	30	76.5	<u>42.2</u>	<u>28.4</u>	<u>21.5</u>
MAE-CT _{aug}	10	77.9	48.8	35.8	28.2

Table 17. Evaluation with linear classifiers trained on ImageNet. We compare different ViT-L/16 models and report accuracy for multiple values of k in the topk-NN lookup. We evaluate on ImageNet-V2, ImageNet-R, ImageNet-Sketch, and ImageNet-A.

Extended results. Table 18 on the next page presents an extended version of the linear probing and k -NN result tables of the main paper. We include results from models that use smaller patches or a higher input resolution.

Method	Architecture	Epochs	Global views	Local views	Teacher	Mask ratio	Probe	k -NN
<i>minimal image augmentations</i>								
SimMIM [84]	ViT-B/16	800	1	-	-	0.5	56.7	-
MAE [37]	ViT-B/16	1600	1	-	-	0.75	68.0	50.0
MAE [37]	ViT-L/16	1600	1	-	-	0.75	76.0	60.6
MAE [37]	ViT-H/14	1600	1	-	-	0.75	77.2	58.9
MAE (reimpl.)	ViT-B/16	800	2	-	-	0.75	66.7	51.1
MAE (reimpl.)	ViT-L/16	800	2	-	-	0.75	75.9	57.6
MAE (reimpl.)	ViT-H/16	800	2	-	-	0.75	78.0	61.1
I-JEPA [4]	ViT-B/16	600	1*	4*	1	*	72.9	-
I-JEPA [4]	ViT-L/16	600	1*	4*	1	*	77.5	-
I-JEPA [4]	ViT-H/14	300	1*	4*	1	*	79.3	-
I-JEPA [4]	ViT-H/16 ₄₄₈	300	1*	4*	1	*	81.1	-
MAE-CT	ViT-B/16	800; 20	2	-	-	0.75; 0	73.5	64.1
MAE-CT	ViT-L/16	800; 20	2	-	-	0.75; 0	80.2	78.0
MAE-CT	ViT-H/16	800; 30	2	-	-	0.75; 0	81.5	79.4
<i>extensive image augmentations</i>								
NNCLR [29]	ViT-B/16	1000	2	-	-	-	76.4	-
MoCo v3 [18]	ViT-B/16	600	2	-	-	-	76.7	-
MoCo v3 [18]	ViT-L/16	300	2	-	-	-	77.6	-
MoCo v3 [18]	ViT-L/7-BN	300	2	-	-	-	81.0	-
MoCo v3 [18]	ViT-H/14	300	2	-	-	-	78.1	-
MoCo v3 [18]	ViT-H/14-BN	300	2	-	-	-	79.1	-
DINO [13]	ViT-S/8	400	2	10	2	-	79.7	78.3
DINO [13]	ViT-B/16	400	2	10	2	-	78.2	76.1
DINO [13]	ViT-B/8	400	2	10	2	-	80.1	77.4
iBOT [91]	ViT-B/16	400	2	10	2	$\approx 0.15^\dagger$	79.5	77.1
iBOT [91]	ViT-L/16	250	2	10	2	$\approx 0.15^\dagger$	81.0	78.0
MSN [3]	ViT-L/7	200	2	10	2	0.7	80.7	-
CMAE [47]	ViT-B/16	1600	1	-	1	0.75	73.9	-
Layer Grafting [51]	ViT-B/16	1600; 300	1; 2	-	-; 2	0.75; 0	77.9	-
Layer Grafting [51]	ViT-L/16	1600; 300	1; 2	-	-; 2	0.75; 0	81.0	-
MAE-CT _{aug}	ViT-B/16	800; 80	2	-	-	0.75; 0	76.9	73.4
MAE-CT _{aug}	ViT-L/16	800; 40	2	-	-	0.75; 0	81.5	79.1
MAE-CT _{aug}	ViT-H/16	800; 40	2	-	-	0.75; 0	82.2	79.8

Table 18. Comparison of linear probing and k -NN accuracies, including results of methods that use smaller patches or higher resolutions. Furthermore, training details are listed. Namely, the training duration, the number of global views, the number of local views (multi-crop), the number of teacher forward passes and the masking ratio.

* I-JEPA uses a multiblock-masking scheme, consisting of one context block and four target blocks (no encoder forward pass) per sample. Thus the effective masking ratio is a result of the size of the context block, the sizes of the target blocks and the overlap between them.

\dagger iBOT applies masking only half of the time during training. If masking is applied the masking ratio is sampled between 0.1 and 0.5.

B.3. Cluster Analysis

Experiment details. The clustering performance metrics in Table 4 of the main paper are obtained by applying k -means to the [CLS] token in the last layer of each ViT encoder. Only for MAE-CT and MAE-CT_{aug} with ViT-B we use the average over the patch tokens of the last encoder layer for clustering. For each method we encoded the validation set of ImageNet and standardized the embedding using its mean and standard deviation. The standardized embedding is then clustered 100 times with mini-batch k -means¹, a mini-batch variant of k -means that scales better with larger data sets [71]. From the 100 runs we selected the one with the lowest k -means loss and calculated the cluster accuracy [86] w.r.t. the 1000 ground truth ImageNet classes. For ImageNet-Dogs15 [14] we performed the same procedure with the number of clusters $k = 15$.

Quantitative results. In Table 19 we show for completeness the best (w.r.t. the lowest k -means loss) clustering performance for ImageNet and in Table 20 we report the average results. For ImageNet-Dogs15 we report the best results in Table 21 and average results in Table 22. In addition to the cluster accuracy (ACC) results presented in the main paper we report the commonly used clustering metrics Normalized Mutual Information (NMI; [63]), Adjusted Mutual Information (AMI; [63]) and Adjusted Rand Index (ARI; [48]) as well. ACC, NMI, AMI and ARI are all multiplied by 100, so they range between 0 and 100, where higher values indicate a better match with the ground truth labels. The ACC standard deviations over the 100 runs are small for ImageNet, ranging from 0.2% to 0.7% and higher for ImageNet-Dogs15, ranging from 0.6% to 4.3%.

Qualitative results. In Figure 8 we show the UMAP [60] plots for the [CLS] token embedding of ImageNet-Dogs15 of MAE vs. MAE-CT for ViT-H. We see that the cluster structure is much more visible for MAE-CT. Figure 9 shows the corresponding confusion matrices, where clusters are matched to the ground truth classes using a variant of the Hungarian algorithm [21]. In Figure 10 we show the corresponding cluster retrievals for MAE vs. MAE-CT where we can see again that the nearest neighbors of k -means cluster centers discovered by MAE-CT are focusing more on the different dog breeds than on the background as in MAE. Additionally, Figure 11 shows three samples of ImageNet and the nearest neighbors for MAE, MAE-CT and MAE-CT_{aug}, respectively.

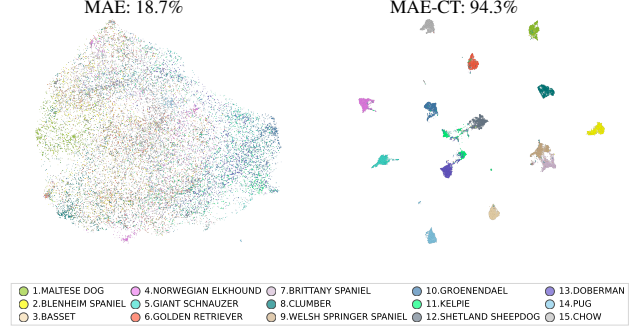


Figure 8. Visualization of UMAP embeddings from the [CLS] token of ViT-H/16 over MAE and MAE-CT with corresponding k -means cluster accuracies (w.r.t. lowest k -means loss) for ImageNet-Dogs15. MAE-CT clearly improves the separation of the 15 classes.

1. MALTESE DOG	277	296	102	44	16	106	152	38	11	6	4	71	3	34	40
2. BLENHEIM SPANIEL	125	166	152	61	37	98	173	102	64	14	14	132	11	63	88
3. BASSET	89	117	249	101	44	73	66	20	83	6	17	217	42	102	74
4. NORWEGIAN ELKHOUND	17	57	140	138	82	96	60	83	78	28	110	167	21	173	50
5. GIANT SCHNAUZER	1	2	47	80	250	4	1	5	51	231	100	93	323	57	55
6. GOLDEN RETRIEVER	65	124	84	106	60	112	133	75	121	17	25	127	24	108	119
7. BRITTANY SPANIEL	92	137	102	126	47	78	179	91	135	10	17	119	19	90	58
8. CLUMBER	198	72	64	90	7	95	209	330	95	3	31	61	7	23	15
9. WELSH SPRINGER SPANIEL	74	87	95	180	51	47	197	76	175	9	36	130	24	72	47
10. GROENENDAEL	2	11	26	69	207	6	3	1	66	106	123	57	237	45	49
11. KELPIE	8	15	79	108	110	16	21	12	99	114	249	122	185	82	80
12. SHETLAND SHEEPDOG	92	164	205	132	64	57	82	24	64	6	8	232	24	92	54
13. DOBERMAN	0	12	85	72	113	19	0	10	84	98	120	101	105	109	65
14. PUG	41	103	258	116	53	44	55	5	51	29	12	208	40	216	69
15. CHOW	39	128	112	48	85	76	51	58	55	47	48	176	29	169	179
	Cluster 1	Cluster 2	Cluster 3	Cluster 4	Cluster 5	Cluster 6	Cluster 7	Cluster 8	Cluster 9	Cluster 10	Cluster 11	Cluster 12	Cluster 13	Cluster 14	Cluster 15
1. MALTESE DOG	277	0	4	0	1	1	0	0	0	0	15	1	0	0	0
2. BLENHEIM SPANIEL	0	124	1	0	0	2	6	1	29	0	9	5	0	0	0
3. BASSET	2	0	125	0	0	5	3	1	11	1	21	0	1	0	0
4. NORWEGIAN ELKHOUND	0	0	0	133	0	3	0	0	0	6	51	10	0	5	0
5. GIANT SCHNAUZER	0	0	0	2	119	1	1	0	0	3	90	2	3	0	0
6. GOLDEN RETRIEVER	0	0	0	0	0	135	0	0	2	1	12	0	0	0	0
7. BRITTANY SPANIEL	0	7	3	0	1	9	1048	4	203	0	21	4	0	0	0
8. CLUMBER	6	1	3	0	2	26	2	119	32	2	23	3	0	2	0
9. WELSH SPRINGER SPANIEL	0	1	0	0	0	1	17	0	134	0	9	2	3	0	0
10. GROENENDAEL	0	0	0	2	1	0	0	0	0	125	37	1	2	0	0
11. KELPIE	0	0	1	2	1	19	1	0	0	12	123	11	20	0	0
12. SHETLAND SHEEPDOG	1	1	1	0	0	3	0	0	3	0	15	176	0	0	0
13. DOBERMAN	0	0	0	0	2	0	0	0	0	0	121	1	176	0	0
14. PUG	0	0	0	0	0	0	0	1	0	0	101	2	0	119	0
15. CHOW	0	0	1	5	0	24	0	0	1	7	10	7	0	0	125
	Cluster 1	Cluster 2	Cluster 3	Cluster 4	Cluster 5	Cluster 6	Cluster 7	Cluster 8	Cluster 9	Cluster 10	Cluster 11	Cluster 12	Cluster 13	Cluster 14	Cluster 15

Figure 9. Confusion matrices w.r.t. the clustering result with lowest k -means loss for MAE (upper) with 18.7% cluster accuracy and MAE-CT (lower) with 94.3% for ViT-H. MAE-CT discovers clusters that correspond well to the ground truth dog breeds.

¹We used the publicly available implementation of scikit-learn [66], see <https://scikit-learn.org/stable/modules/generated/sklearn.cluster.MinibatchKMeans.html>.

Method	ViT-B/16				ViT-L/16				ViT-H/16			
<i>minimal image augmentations</i>												
	ACC	NMI	AMI	ARI	ACC	NMI	AMI	ARI	ACC	NMI	AMI	ARI
MAE (reimpl.)	13.8	51.4	20.7	4.4	14.3	51.9	22.8	4.6	11.1	48.2	17.1	2.9
MAE-CT	35.3	68.2	45.8	19.7	54.9	80.6	66.8	34.5	58.0	81.8	69.3	36.8
<i>extensive image augmentations</i>												
Moco v3 [18]	43.0	73.0	55.5	23.1	-	-	-	-	-	-	-	-
DINO [13]	48.0	77.9	63.2	31.2	-	-	-	-	-	-	-	-
MSN [3]	54.2	79.9	66.6	30.2	45.4	76.2	63.2	19.5	-	-	-	-
iBOT [91]	50.0	79.1	64.9	32.6	52.0	80.5	66.8	35.0	-	-	-	-
MAE-CT _{aug}	46.2	76.0	59.0	29.8	56.9	81.7	68.4	40.5	54.8	81.1	67.6	38.9

Table 19. Best cluster performance of k -means (w.r.t. lowest k -means loss) over 100 runs for ImageNet validation set.

Method	ViT-B/16				ViT-L/16				ViT-H/16			
<i>minimal image augmentations</i>												
	ACC	NMI	AMI	ARI	ACC	NMI	AMI	ARI	ACC	NMI	AMI	ARI
MAE (reimpl.)	13.5	51.0	20.8	4.3	13.9	51.2	22.9	4.5	10.6	47.5	17.0	2.7
MAE-CT	35.0	68.0	45.4	19.5	54.1	80.6	66.9	34.7	57.1	81.7	69.2	35.6
<i>extensive image augmentations</i>												
Moco v3 [18]	41.5	72.4	55.2	21.2	-	-	-	-	-	-	-	-
DINO [13]	46.5	77.3	62.7	29.0	-	-	-	-	-	-	-	-
MSN [3]	52.7	79.4	65.9	28.8	43.6	75.6	62.7	18.6	-	-	-	-
iBOT [91]	49.2	78.7	64.6	31.6	51.2	80.1	66.4	34.1	-	-	-	-
MAE-CT _{aug}	45.3	75.7	58.8	28.6	55.6	81.4	68.0	39.4	54.7	80.8	67.3	37.8

Table 20. Average cluster performance of k -means over 100 runs for ImageNet validation set.

Method	ViT-B/16				ViT-L/16				ViT-H/16			
<i>minimal image augmentations</i>												
	ACC	NMI	AMI	ARI	ACC	NMI	AMI	ARI	ACC	NMI	AMI	ARI
MAE (reimpl.)	16.0	8.1	7.9	3.2	18.9	12.8	12.6	5.2	18.7	11.7	11.6	4.7
MAE-CT	70.8	69.1	69.0	54.3	84.2	85.6	85.6	76.4	94.3	90.4	90.4	87.9
<i>extensive image augmentations</i>												
Moco v3 [18]	72.7	71.9	71.8	59.3	-	-	-	-	-	-	-	-
DINO [13]	79.0	78.9	78.9	69.4	-	-	-	-	-	-	-	-
MSN [3]	81.0	83.6	83.6	73.7	83.3	84.2	84.2	75.9	-	-	-	-
iBOT [91]	77.2	78.8	78.8	68.5	69.4	72.8	72.8	59.9	-	-	-	-
MAE-CT _{aug}	78.1	77.4	77.3	65.0	84.8	87.8	87.8	81.1	83.7	86.5	86.4	79.3

Table 21. Best cluster performance of k -means (w.r.t. lowest k -means loss) over 100 runs for ImageNet-Dogs15.

Method	ViT-B/16				ViT-L/16				ViT-H/16			
<i>minimal image augmentations</i>												
	ACC	NMI	AMI	ARI	ACC	NMI	AMI	ARI	ACC	NMI	AMI	ARI
MAE (reimpl.)	15.7	8.5	8.3	3.3	18.5	12.3	12.1	5.2	17.6	11.7	11.5	4.8
MAE-CT	67.9	69.2	69.2	53.5	79.9	83.4	83.4	72.7	87.4	88.2	88.2	82.1
<i>extensive image augmentations</i>												
Moco v3 [18]	66.7	68.8	68.8	54.2	-	-	-	-	-	-	-	-
DINO [13]	71.4	75.2	75.2	62.2	-	-	-	-	-	-	-	-
MSN [3]	79.7	82.4	82.3	72.2	79.5	82.9	82.9	72.5	-	-	-	-
iBOT [91]	75.2	78.6	78.6	66.9	64.8	70.5	70.4	55.4	-	-	-	-
MAE-CT _{aug}	71.7	74.7	74.7	60.3	84.7	86.5	86.4	79.1	83.2	86.0	86.0	78.2

Table 22. Average cluster performance of k -means over 100 runs for ImageNet-Dogs15.

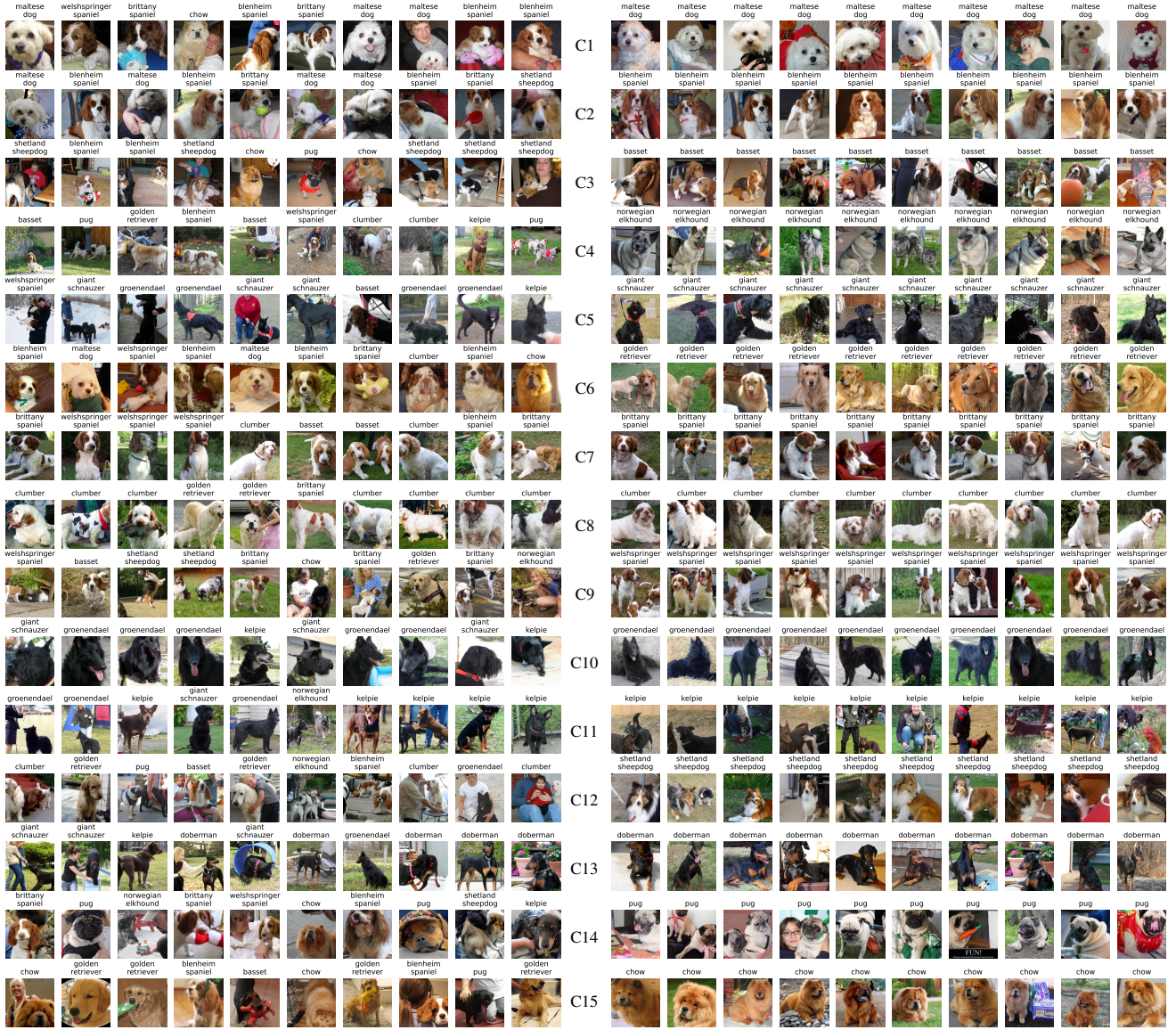


Figure 10. **Cluster retrieval**: Ten nearest neighbors per k -means cluster center for MAE (left) and MAE-CT (right). Each row corresponds to one cluster (C1 to C15) found in the [CLS] token embedding of ViT-H for Imagenet-Dogs15. MAE clusters correspond more to background and surface characteristics like color, while MAE-CT found clusters that correspond to the 15 dog breeds. The mapping from each cluster to dog breed for MAE-CT can be found in the confusion matrix in Figure 9, e.g. the first row is *cluster 1* (C1) and corresponds to the class *maltese dog*. Additionally, the ground truth label is shown on top of each image (best viewed with zooming in).



Figure 11. Nearest neighbor retrieval: Nearest neighbors for three different sample images (first column) for MAE, MAE-CT and MAE-CT_{aug}. The NNs are computed by calculating the [CLS] token embedding of a ViT-H for all images in the ImageNet validation set and searching for the most similar embeddings in terms of cosine similarity. The first and the second example images (*partridge* and *strawberry*) show that the NNs of the MAE are similar in the context in which the image was taken but almost never contain the correct class. However, the NNs of the MAE-CT and the MAE-CT_{aug} are images of the same class as the example images. The third sample image is labeled as *viaduct*, but the image clearly also contains a *steam locomotive*. The NNs of the MAE all belong to different classes, which shows that the MAE has not captured the semantics of a *viaduct* or a *steam locomotive*. The NNs of the MAE-CT and the MAE-CT_{aug} are all of the same class, but it is either the *steam locomotive* or the *viaduct*. All NNs of MAE-CT_{aug} are images of other *viaducts* recognizable by their characteristic shape, showing that the augmentations of MAE-CT_{aug} result in a representation that focuses more on shapes and less on characteristic colors, like black locomotives.